Report 76-0137

DAVID W. TAYLOR NAVAL SHIP RESEARCH AND DEVELOPMENT CENTER

Bethesda, Md. 20084

EXPERIMENTAL INVESTIGATION OF THE EFFECT OF PROPELLER BLADE PITCH ON PROPELLER-PRODUCED UNSTEADY BEARING FORCES AND MOMENTS

EXPERIMENTAL INVESTIGATION OF THE EFFECT OF PROPELLER BLADE PITCH ON PROPELLER-PRODUCED UNSTEADY BEARING FORCES AND MOMENTS

by

D.T. Valentine and R.D. Kader

SHIP PERFORMANCE DEPARTMENT
RESEARCH AND DEVELOPMENT REPORT

December 1976

Report 76-0137

MAJOR DTNSRDC ORGANIZATIONAL COMPONENTS

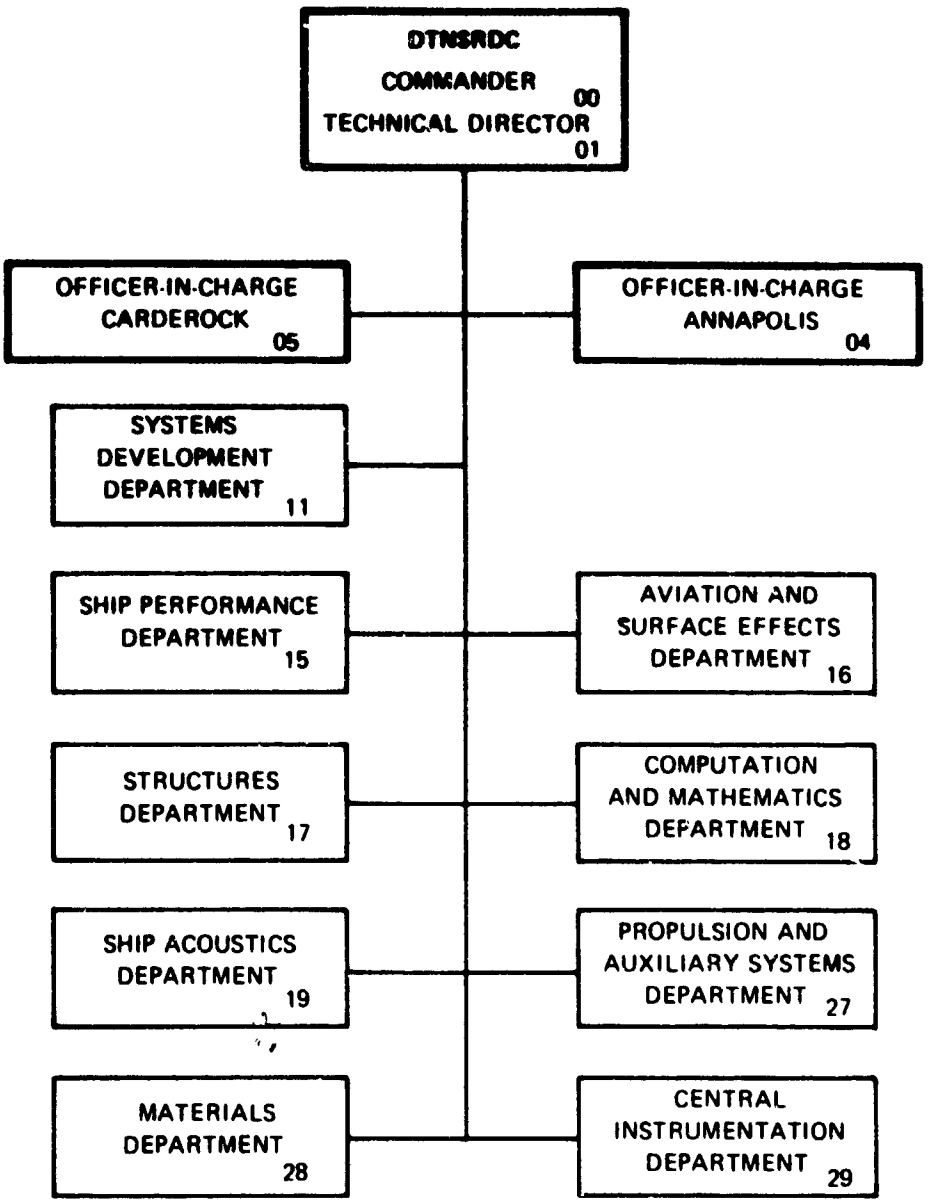

DTNSRDC ISSUES THREE TYPES OF REPORTS

(1) DTNSRDC REPORTS, A FORMAL SERIES PUBLISHING INFORMATION OF PERMANENT TECHNICAL VALUE, DESIGNATED BY A SERIAL REPORT NUMBER.

(2) DEPARTMENTAL REPORTS, A SEMIFORMAL SERIES, RECORDING INFORMATION OF A PRELIMINARY OR TEMPORARY NATURE, OR OF LIMITED INTEREST OR SIGNIFICANCE, CARRYING A DEPARTMENTAL ALPHANUMERIC IDENTIFICATION.

(3) TECHNICAL MEMORANDA, AN INFORMAL SERIES, USUALLY INTERNAL WORKING PAPERS OR DIRECT REPORTS TO SPONSORS, NUMBERED AS TM SERIES REPORTS; NOT FOR GENERAL DISTRIBUTION.

UNCLASSIFIED

SECURITY CLASSIFICATION OF THIS PAGE (When Data Entered)

REPORT DOCUMENTATION PAGE

READ INSTRUCTIONS BEFORE COMPLETING FORM

1 REPORT NUMBER: DTNSRDC [redacted]-76-0137

2 GOVT ACCESSION NO.

3 RECIPIENT'S CATALOG NUMBER

4 TITLE (and Subtitle): EXPERIMENTAL INVESTIGATION OF THE EFFECT OF PROPELLER BLADE PITCH ON PROPELLER-PRODUCED UNSTEADY BEARING FORCES AND MOMENTS

5 TYPE OF REPORT & PERIOD COVERED

6 PERFORMING ORG. REPORT NUMBER

7 AUTHOR(s): D.T. Valentine [redacted] R.D. Kader

8 CONTRACT OR GRANT NUMBER(s)

9 PERFORMING ORGANIZATION NAME AND ADDRESS: David W. Taylor Naval Ship Research and Development Center, Bethesda, Maryland 20084

10 PROGRAM ELEMENT, PROJECT, TASK AREA & WORK UNIT NUMBERS: (See reverse side)

11 CONTROLLING OFFICE NAME AND ADDRESS: Naval Sea Systems Command, Ship Silencing Division (037), Washington, D.C. 20362

12 REPORT DATE: Dec[redacted]76

13 NUMBER OF PAGES: 60

14 MONITORING AGENCY NAME & ADDRESS (if different from Controlling Office)

15 SECURITY CLASS. (of this report): UNCLASSIFIED

15a DECLASSIFICATION/DOWNGRADING SCHEDULE

16 DISTRIBUTION STATEMENT (of this Report)

APPROVED FOR PUBLIC RELEASE: DISTRIBUTION UNLIMITED

17 DISTRIBUTION STATEMENT (of the abstract entered in Block 20, if different from Report)

18 SUPPLEMENTARY NOTES

19 KEY WORDS (Continue on reverse side if necessary and identify by block number)

Pitch effects
Vibratory forces

20 ABSTRACT (Continue on reverse side if necessary and identify by block number)

Experimental results are presented to show the effect of pitch-diameter ratio on propeller-produced unsteady loads. Eight three-bladed propellers with changes of equal increments of pitch resulting in pitch-diameter ratios from 0.58 to 1.75 were tested in three-cycle and four-cycle wake screens. The data indicated that, in general, for the same thrust loading coefficient C_{Th}, the unsteady thrust and bending moments tend to decrease with increasing

(Continued on reverse side)

DD FORM 1 JAN 73 1473 EDITION OF 1 NOV 65 IS OBSOLETE
S/N 0102-014-6601

UNCLASSIFIED

SECURITY CLASSIFICATION OF THIS PAGE (When Data Entered)

(Block 10)
62754N
SF 43 452 702
16079
1-1544-259

(Block 20 continued)
pitch whereas the torque increases and the side forces change negligibly. However, it is impracticable to reduce unsteady thrust by altering pitch. For low thrust loading coefficients, e.g., C_{Th} = 0.51, optimum propeller efficiencies were obtained with the higher pitch-diameter ratios. For high thrust loading coefficients, e.g., C_{Th} = 1.53, the optimum propeller efficiencies were obtained at the lower pitch ratios. However, the alternating forces did not vary much for the high as for the low C_{Th} designs and the optimum efficiency pitch ratio was near the optimum unsteady loading pitch ratio. Consequently, propeller designs for optimum efficiencies are the most appropriate selections with regards to pitch-diameter ratio.

Results are presented for the six components of unsteady loading divided by the appropriate steady loading. As an example, the thrust and torque variations were as follows. For a thrust loading coefficient of 0.51 and a change in pitch-diameter ratio from 0.58 to 1.75, the alternating thrust ratio ($\hat{T}$ / $\bar{T}$) changed from 0.74 to 0.40, and the alternating torque ratio ($\hat{Q}$ / $\bar{Q}$) changed from 0.40 to 0.31. For a thrust loading coefficient of 1.53 and the same change in pitch-diameter ratio, $\hat{T}$ / $\bar{T}$ changed from 0.26 to 0.2 and there was only a negligible change in $\hat{Q}$ / $\bar{Q}$.

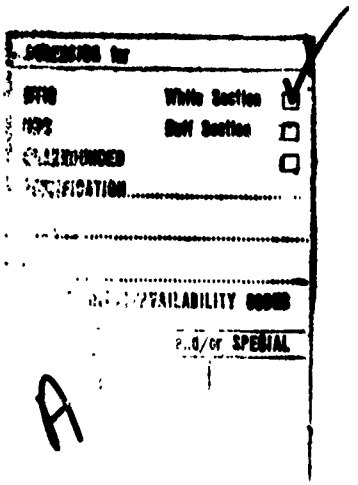

TABLE OF CONTENTS

LIST OF FIGURES

LIST OF TABLES

NOTATION

a_n	Fourier cosine coefficients of longitudinal wake velocity
b_n	Fourier sine coefficients of longitudinal wake velocity
$c(r)$	Chord length
C_{Th}	$T / (1/2\rho\pi V_A^2 R^2)$ Thrust loading coefficient
D	Propeller diameter
EAR	Expanded area ratio, expanded blade area divided by disk area
$\tilde{F}_H$	Amplitude of harmonic of horizontal side force
$\tilde{F}_V$	Amplitude of harmonic of vertical side force
$\tilde{F}_1$	Amplitude of harmonic of lagging component of side force rotating with propeller
$\tilde{F}_2$	Amplitude of harmonic of leading component of side force rotating with propeller
J	V_A/nD, advance coefficient
$\tilde{K}_F$	$\tilde{F}/\rho n^2 D^4$, force coefficient based upon amplitude of harmonic of force
$\tilde{K}_M$	$\tilde{M}/\rho n^2 D^5$, moment coefficient based upon amplitude of harmonic of moment
K_Q, $\bar{K}_Q$	$Q/\rho n^2 D^5$, torque coefficient based upon steady component of torque
$\tilde{K}_Q$	$\tilde{Q}/\rho n^2 D^5$, torque coefficient based upon amplitude of harmonic of torque
K_T, $\bar{K}_T$	$T/\rho n^2 D^4$, thrust coefficient based upon steady component of thrust

$\tilde{K}_T$	$\tilde{T}/\rho n^2 D^4$, thrust coefficient based upon amplitude of harmonic of thrust
k	Order of blade harmonic
L(r)	Unsteady lift on a blade element
$\tilde{M}_H$	Amplitude of harmonic of horizontal bending moment
$\tilde{M}_V$	Amplitude of harmonic of vertical bending moment
$\tilde{M}_1$	Amplitude of harmonic of leading component of bending moment rotating with propeller
$\tilde{M}_2$	Amplitude of harmonic of lagging component of bending moment rotating with propeller
n	Order of shaft harmonic
n	$2\pi\Omega$, in revolutions per second
$\vec{n}$	Normal to helicoidal surface at loading point
$\vec{n}'$	Normal to helicoidal surface at control point
P	Propeller pitch
p	Perturbation pressure
$Q, \bar{Q}$	Steady component of torque
$\tilde{Q}$	Harmonic amplitude of torque
R	Radius of propeller
Re[]	Real part of []
R_n	Reynolds number for propeller; $c_{0.7}\left(\frac{\sqrt{V_A^2 + (0.7\ \pi nD)^2}}{\nu}\right)$

r	Radial coordinate of control point
r_h	Radius of hub
$T, \bar{T}$	Steady component of thrust
$\tilde{T}$	Amplitude of harmonic of thrust
t	Time
$V(r,\phi)$	Local inflow velocity to propeller plane
V_A	Speed of advance
$V_L(r,\phi)$	Local longitudinal inflow velocity to propeller plane
$V_N^n(r)$	Fourier coefficients of wake velocity normal to the blade
V_{VM}	Volume mean velocity into propeller disk
x	Longitudinal coordinate of control point
x,r,ϕ	Cylindrical coordinate system of control point
Z	Number of blades
β	Advance angle of a propeller blade section
η_o	Efficiency of propeller in open water
θ	Angular coordinate of loading point; angular coordinate in propeller disc, positive clockwise looking forward
θ_b	Propeller angular position relative to position where $\tilde{M}_l = \tilde{M}_V$
θ_p	Propeller geometry pitch angle
ρ	Mass density of fluid
Ω	Angular velocity of propeller in radians per second

ABSTRACT

Experimental results are presented to show the effect of pitch-diameter ratio on propeller-produced unsteady loads. Eight three-bladed propellers with changes of equal increments of pitch resulting in pitch-diameter ratios from 0.58 to 1.75 were tested in three-cycle and four-cycle wake screens. The data indicated that, in general, for the same thrust loading coefficient C_{Th}, the unsteady thrust and bending moments tend to decrease with increasing pitch whereas the torque increases and the side forces change negligibly. However, it is impracticable to reduce unsteady thrust by altering pitch. For low thrust loading coefficients, e.g., $C_{Th} = 0.51$, optimum propeller efficiencies were obtained with the higher pitch-diameter ratios. For high thrust loading coefficients, e.g., $C_{Th} = 1.53$, the optimum propeller efficiencies were obtained at the lower pitch ratios. However, the alternating forces did not vary much for the high as for the low C_{Th} designs and the optimum efficiency pitch ratio was near the optimum unsteady loading pitch ratio. Consequently, propeller designs for optimum efficiencies are the most appropriate selections with regards to pitch-diameter ratio.

Results are presented for the six components of unsteady loading divided by the appropriate steady loading. As an example, the thrust and torque variations were as follows. For a thrust loading coefficient of 0.51 and a change in pitch-diameter ratio 0.58 to 1.75, the alternating thrust ratio $(\tilde{T} / \bar{T})$ changed from 0.74 to 0.40, and the alternating torque ratio $(\tilde{Q} / \bar{Q})$ changed from 0.40 to 0.31. For a thrust loading coefficient of 1.53 and the same change in pitch-diameter ratio, $(\tilde{T} / \bar{T})$ changed from 0.26 to 0.2 and there was only a negligible change in $(\tilde{Q} / \bar{Q})$.

ADMINISTRATIVE INFORMATION

This project was sponsored by the Ship Silencing Division (037) of the Naval Sea Systems Command under Program Element 62754N, and Task SF 43 452 702. The work was performed at the David W. Taylor Naval Ship Research and Development Center (DTNSRDC) under Task 16079, Work Unit 1-1544-259.

INTRODUCTION

The unsteady forces and moments produced by operation of a propeller in the wake of a ship are of fundamental importance in the analysis of machinery and hull vibration. The circumferentially nonuniform inflow into the propeller subjects each blade section to periodic variations in its inflow velocity and angle of attack, resulting in undesirable fluctuations in the propeller loading. These propeller-produced fluctuating forces and moments (unsteady bearing forces and moments) are transmitted from the propeller through its shaft and bearings to the machinery and other parts of the hull structure. (Propeller-generated pressure fluctuations are also transmitted through the water to the ship hull and can cause the hull to vibrate; however, that type of vibration is not considered in this report.) Severe vibration problems can result if the alternating forces are large. In addition, since vibration problems increase with increasing speed and power and since the trend of advancing ship technology is toward increased speed and power, the unsteady forces produced by the propeller are of considerable interest to the designers of ships and propellers. Therefore, it has become increasingly important to design propellers with blade shapes selected to reduce the alternating forces. This requires information on how the various geometric parameters of a propeller influence the magnitude of the alternating forces and moments.

The present investigation was conducted as part of a continuing effort at the David W. Taylor Naval Ship Research and Development Center (DTNSRDC) to evaluate the effects of various parameters, e.g., wake velocity distribution, propeller blade skew, blade warp, blade width, pitch-ratio, etc., on the propeller-generated unsteady bearing forces and moments. The objective of this investigation was to determine experimentally the effect of pitch-diameter ratio on the alternating forces produced by a propeller operating in a wake. The results indicate that, in general, the higher the pitch in a given design problem, the lower the blade frequency thrust and the higher the blade frequency torque. In addition, the propeller side

forces tend to increase slightly and the bending moments decrease with an increase in pitch. The blade frequency torque results disagree with analytical calculations by Boswell and Miller[1] of the effect of pitch on propeller-produced unsteady thrust and torque. In their parametric investigation of various propeller geometrical parameters, they considered the effect of pitch analytically. Their calculations were made with an early version of a propeller unsteady forces prediction computer program developed at the Stevens Institute of Technology (SIT) and reported by Tsakonas, Breslin, and Miller.[2] No comparisons with analytical predictions based on this program, other than the Boswell and Miller results, are presented herein. The numerical analysis procedure has been superseded by a more exact approach, also developed at SIT, as reported by Tsakonas, Jacobs, and Ali.[3] The continuing development of the analytical procedures has created an obvious need for experimental data for comparison purposes. It is in this spirit that the results of the present investigation are reported.

Eight 1-ft (0.305-m)-diameter, three-bladed propellers with expanded area ratios of 0.54 and pitch-diameter (P/D) ratios varying from 0.58 to 1.75 were tested in three-cycle and four-cycle wake screens. The six components of the alternating propeller forces and moments were measured in the closed-jet test section of the 24-in. variable-pressure water tunnel at DTNSRDC. The unsteady thrust decreased and the unsteady torque increased by factors of 1.9 and 1.4, respectively, for a thrust loading coefficient

---

[1]Boswell, R.J. and M.L. Miller, "Unsteady Propeller Loading - Measurement, Correlation with Theory, and Parametric Study," NSRDC Report 2625 (Oct 1968). A complete listing of references is given on page 48.

[2]Tsakonas, S. et al., "Correlation and Application of an Unsteady Flow Theory for Propeller Forces," Transactions of the Society of Naval Architects and Marine Engineers, Vol. 75, pp. 158-193 (1967).

[3]Tsakonas, S. et al., "An Exact Linear Lifting-Surface Theory for a Marine Propeller in a Nonuniform Flow Field," Stevens Institute of Technology DL Report 1509 (Feb 1972).

C_{Th} = 0.51 and a change in P/D ratio from 0.58 to 1.75. The unsteady thrust decreased and the unsteady torque increased by factors of 1.8 and 1.9, respectively, for a thrust loading coefficient C_{Th} = 1.53 and a change in P/D ratio from 0.58 to 1.75. The optimum P/D ratios for the thrust loading coefficients C_{Th} = 0.51 and 1.53 were approximately equal to 1.45 and 1.1, respectively. The observed trends are of interest in the design problem. For instance, varying the P/D ratio as a means of reducing alternating thrust is not practicable because (1) designs selected on the basis of optimum propeller efficiency are near optimum with regard to the pitch that affects the alternating forces production; (2) the alternating torque tends to increase with pitch; and (3) it has been demonstrated that other blade shape changes, e.g., skew[1,4,5] and warp[6] cause greater changes in the alternating forces produced by the propeller than the changes attributable to pitch and measured in this experiment.

METHOD AND PROCEDURE

PROPELLER MODELS

The present investigation required a fairly large number of propellers. Eight commercially available models, designated the M-P design series by the manufacturer, were purchased from Michigan Wheel. The only change in the catalog specifications was an increase in the diameter of the stock hub as necessary to fit the existing dynamometer mount. The adequacy of

---

[4]Cumming, R.A., et al., "Highly Skewed Propellers," Transactions of the Society of Naval Architects and Marine Engineers, Vol. 80, pp. 98-135 (1972).

[5]Valentine, D.T. and F.J. Dashnaw, "Highly Skewed Propellers for San Clemente Class Ore/Bulk/Oil Carrier Design Considerations, Model and Full-Scale Evaluation," Proceedings of the First Ship Technology and Research (STAR) Symposium, Washington, D.C. (Aug 1975).

[6]Nelka, J.J., "Experimental Evaluation of a Series of Skewed Propellers with Forward Rake: Open-Water Performance, Cavitation Performance, Field-Point Pressures, and Unsteady Propeller Loading," DTNSRDC Report 4113 (Jul 1974).

commercially available propellers for the present investigation was verified by comparing the present results with those of Boswell and Miller,[1] as discussed later.

All eight propellers had a diameter of 1 ft (30.5 cm), a blade area ratio of 0.54, three blades, and zero skew. Thus the propellers differed only in pitch (17.78, 22.86, 27.94, 33.02, 38.1, 43.18, 48.26, and 53.34 cm). This range of P/D ratios (from 0.58 to 1.75) was selected because most practical designs fall within it. Table 1 summarizes the geometrical particulars of the propellers, Figure 1 illustrates the typical shape of the series, and Figure 2 shows their open-water characteristics.*

TEST FACILITY AND EQUIPMENT

The present experiments were performed in the DTNSRDC 24-in. variable-pressure water tunnel, a recirculating tunnel with provisions for mounting wake simulation grids into its 27-in. (68.6-cm)-diameter closed-jet test section.** Three-bladed propellers had been selected for the investigation because of the availability of wake screens for inducing three-cycle and four-cycle wakes. The wire mesh screens had been constructed[1] by using a base screen of 0.009-in. (0.023-cm)-diameter wire (16 per inch or 6.3 per centimeter) and a single overlay screen of 0.015-in. (0.038-cm)-diameter wire (18 per inch or 7.1 per centimeter) in the high-wake region. The overlay screen was oriented so that its wires intersected those of the base screen at 45 deg (0.785 rad). Since each model was located 2 1/2 propeller

---

*Code 1524 at DTNSRDC used the deep-water basin and standardized methods to determine the first-quadrant open-water characteristics of the eight propellers. A gravity dynamometer installed in the propeller boat was utilized to measure thrust and torque. The propellers were run at several shaft speeds and speeds of advance V_A which resulted in Reynolds numbers on the order of 5×10^5 throughout the range of design interest. The shaft speed and speed of advance were measured to within ±0.01 rps (±0.06 rad/s) and ±0.001 fps (±0.003 m/s), respectively. The thrust and torque for a given advance coefficient were reproducible to better than 2 percent in repetitive experiments.

**The facility is termed the 24-in. tunnel because of the 24-in. diameter of the nozzle exit for the open-jet test section.

diameters downstream, it is believed that its presence did not alter the flow over the wires. Moreover, there was only negligible unsteady interaction between the walls of the test section and each propeller.

The three-cycle wake screen produced a nonuniform inflow with a dominant third harmonic and caused the propellers to develop large blade frequency thrust and torque. The four-cycle wake screen produced a nonuniform inflow with a dominant fourth harmonic and caused the propellers to develop large blade frequency side forces and bending moments. These wake-producing screens were oriented in the tunnel ahead of the propellers; see Figures 3 and 4. The velocity field into the propeller plane produced by the screens had previously been measured with a pitot rake; see Miller and Boswell.[1] Their results were as follows. The circumferential variations in the longitudinal velocity can be expressed as

$$V_L(r,\theta) = V_L(r) + \sum_{n=1}^{\infty} V_L^n(r) \sin(n\theta + \phi_w^n) \qquad (1)$$

where

$V_L(r,\theta)$ = local longitudinal inflow velocity to the propeller plane

$V_L^n(r)$ = Fourier coefficient of the nth harmonic of the circumferential variation in the longitudinal wake velocity

θ = angular coordinate about the shaft axis, positive clockwise looking upstream ($\theta = 0$ for vertical upward)

ϕ_w^n = phase angle of the nth harmonic of the wake

The volume mean velocity over the propeller disk is defined as

$$V_{vm} = \int_0^{2\pi} d\theta \int_{r_h}^{R} r\,dr \frac{V_L(r,\theta)}{2\pi\,(R^2-r_h^2)} \qquad (2)$$

where

V_{vm} = volume mean velocity into the propeller disk

R = radius of the propeller

r_h = radius of the hub

The phase angles and nondimensionalized amplitudes of the first 15 harmonics as defined by Equations (1) and (2) are presented in Tables 2 and 3 for the three- and four-cycle screens, respectively. The amplitudes of the principal harmonics for each screen are presented graphically in Figures 5 and 6. The phase angles are relative to the radial line directed vertically upward from the propeller axis. The relation of the zero phase position in the propeller disk, namely, the upward vertical, corresponds to $\theta = 0$ in the screen plane, as shown in Figures 3 and 4. Therefore, in the special case of an almost purely sinusoidal variation in velocity distribution with negligible differences in phase (radially), the sinusoidal alternating forces and moments can be interpreted as leading or lagging the corresponding frequency components of the longitudinal velocity at the radial line through the midchord of the root section of a propeller blade. This approach in interpretation was followed by Boswell and Miller[1] and explains why the phase angles reported herein are referred to as leading sines; however, this interpretation is not generally applicable to any wake.

EXPERIMENTAL DETERMINATION OF UNSTEADY LOADING

The propeller series was run in both the three- and four-cycle wake patterns. Since the mean tunnel speed could not be measured directly, a thrust identity to open-water results was used to determine the advance coefficients. This assumes that the advance coefficient was the same as that which would have resulted for the same thrust coefficient in the open-water experiments. The shaft speed was set to 12 or 15 rev/s (75.4 or 94.2 rad/s, respectively), depending on the pitch of the propeller and the desired test condition. This provided Reynolds numbers varying from 1.332 to 1.426 x 10^6 for Propellers 4588 to 4591 ($0.58 \leq P/D \leq 1.08$) and from 1.10 to 1.221 x 10^6 for Propellers 4592 to 4595 ($1.25 \leq P/D \leq 61.75$).

Figure 7 presents typical signals from the six-component balance in the three-cycle wake and Figure 8 typical signals in the four-cycle wake. One propeller revolution constituted the distance between the pulses in the upper trace as generated by the single-tooth gear. These signals were recorded on magnetic tape for subsequent computer analysis, and the major harmonic components of each signal were read from the on-the-spot analysis system. All six components of force presented in this report were obtained from computer analysis. The experimentally determined amplitudes of the blade frequency harmonic of all six loading components were accurate within ±5 percent.[7]

INSTRUMENTATION AND DATA ANALYSIS

The six components of unsteady loading were measured by a six-component dynamometer, and a sting-mounted balance with semiconductor strain gages was utilized for the sensing elements. The dynamometer assembly electrical arrangement and the experimental procedure are described in Miller.[7] The strain gage balance was mounted on a stiff sting attached to a flywheel and the whole assembly ran on soft-mounted bearings and was driven through

---

[7] Miller, M.L., "Experimental Determination of Unsteady Propeller Forces," Seventh ONR Symposium on Naval Hydrodynamics, DR-148, pp. 255-289 (Aug 1968).

a soft coupling. This type of mounting was selected to isolate the system from the vibrations of the tunnel; it was small enough to cause little disturbance of the tunnel flow. The totally submerged dynamometer was driven by a 10-hp, d-c motor through an external slipring, shaft, and amplifier housing. The hollow connecting shaft carried the signal cables and passed through a stuffing tube as it entered the tunnel. Before being taken from the shafting, the a-c signals were amplified with solid-state preamplifiers to improve the signal-to-noise ratio.

In order to be useful over the range of test conditions, the dynamometer should have a flat frequency response extending from the lowest shaft frequency of around 10 Hz to several times the highest propeller blade frequency of 400 Hz. The system was represented by lumped parameters, and two principal resonances were determined for each component by means of a vibration analysis. The lower resonance appeared at around 6 Hz and was caused by vibration of sting and balance assembly as a rigid mass on the soft bearing supports. The second resonance at about 450 Hz was the first bending mode due to the mass of the propeller and the spring of the measuring elements.

The balance was calibrated both statically and dynamically. The static calibrations were performed for the balance alone outside the tunnel; the sensitivity of each transducer to the forces applied in axial, torsional, transverse, and bending modes was determined in increments over the input force range. The results indicated only two significant interactions: (1) a small effect of torque on the thrust readings and (2) some effect of bending moment on the output of the side-force gages in the same plane. The dynamic calibration was performed after assembly in the tunnel and consisted of exciting the measuring system with a known force in increments of driving frequency over a broad frequency range. This procedure was carried out to establish the sensitivity in the dynamic response of each transducer over the desired range of measuring frequency.

The sign convention in this report was the same as used by Miller[7] and is presented in Figure 9. The balance was designed to measure force and

moment along a pair of orthogonal axes by means of sensors which rotated with the propeller and allowed the related transverse force and bending-moment vectors to be measured. At any propeller angle θ_b, the forces and moments with respect to the fixed axes are:

$$\tilde{M}_V = \tilde{M}_1 \cos \theta_b + \tilde{M}_2 \sin \theta_b$$

$$\tilde{M}_H = -\tilde{M}_1 \sin \theta_b + \tilde{M}_2 \cos \theta_b$$

$$\tilde{F}_V = \tilde{F}_1 \cos \theta_b - \tilde{F}_2 \sin \theta_b$$

$$\tilde{F}_H = \tilde{F}_1 \sin \theta_b + \tilde{F}_2 \cos \theta_b$$

where $\tilde{M}_1$, $\tilde{M}_2$, $\tilde{F}_1$, and $\tilde{F}_2$ are the moments and forces with respect to the rotating coordinate system.

Figure 10 is a block diagram of the instrumentation used with the dynamometer. Power was supplied to the strain-gage bridges for thrust, torque, side force, and bending moment by four separately adjustable power supplies. The a-c output signals were separated from the steady signals and amplified before leaving the rotating shaft through the sliprings and brushes. Outside the shaft, the a-c signals were sent through another set of amplifiers and a set of attenuators to adjust the signals to the proper level for the tape recording and analyses. The signals were constantly monitored by an oscilloscope, and photographic records were made of the waveforms when the signal was recorded on tape. A one pulse per revolution was also recorded on tape for phase reference along with 60 pulses per revolution to control the analog-to-digital conversion. A digital time code was also recorded on the tape to identify the data and permit the use of an automatic tape-search unit during digitalization. The d-c signals representing the steady components were read on a direct-current electronic voltmeter.

On-the-spot analysis of the signal was carried out by utilizing a two-channel, constant-bandwidth, wave analyzer consisting of a common local oscillator, two mixers, and two crystal filters matched for frequency and phase. The single-tooth pulse was fed into one channel as a phase reference. This pulse contained strong harmonics of the shaft frequency in phase with each other because the pulse was narrow and symmetrical. An oscilloscope enabled the analyzer to be tuned to a desired harmonic of any one of the unsteady signals and the reference signal which had a fixed relationship to the angular position of the propeller. The amplitude of the unsteady signal was measured by a voltmeter, and the phase angle was measured by sending the two signals through a phase meter. All six components were measured by switching the analyzer and multipling by the calibration matrix with side forces and bending moments resolved into vertical and horizontal components by hand calculation.

The magnetic pickup used to sense the position of the single-tooth gear was located in the upward vertical position. The single-tooth gear was so mounted on the shaft that it was in line with the midchord of the reference blade root section. Therefore, the single-tooth signal indicated when the reference blade was in the 0-deg, upward vertical position, i.e., the reference position for the sinusoidal variations in the six components of the propeller unsteady forces is the upward vertical.

The digital analysis was performed by using an Interdata minicomputer to average the signals over an entire run and to multiply the averaged signals by a 6x6 calibration matrix to obtain values of thrust, torque, side forces, and bending moments in pounds and pound-feet. The computer then resolved the rotating side force and bending moment vectors into vertical and horizonal components and harmonically analyzed the signal to provide the steady and higher harmonic amplitudes and the phase angles relative to the propeller position at which the single-tooth pulse was generated.

RESULTS

As already shown in Figure 2, the results of open-water experiments indicated that the pitch for some of the propellers was not precisely correct because the open-water curves were not equally spaced with respect to a line perpendicular to the slope. The observed differences were attributed to allowable commercial tolerances during the commercial manufacturing process. It is felt that such deviations among the propellers in the series did not significantly alter the trends observed in the water-tunnel experiments, as indicated by the fluctuation forces and moments presented next.

Figures 11-18 give the unsteady loading data for the series of propellers selected to investigate the effect of pitch on propeller-produced unsteady loading. Figures 11 and 12 respectively show the nondimensionalized unsteady thrust and torque for the three-cycle wake experiments. The trends indicated that the unsteady thrust and torque increase with increasing advance coefficient. This increase is mainly due to the increase in the circumferential velocity variation which is proportional to the mean velocity. Figures 13 and 14 present the corresponding phase angles for the unsteady thrust and torque. The phase angles given in the figures are defined as follows. Let ϕ_F be the phase angle given by

$$\tilde{F} = |\tilde{F}| \sin (n\theta + \phi_F)$$

where $\tilde{F}$ represents any of the six components of the unsteady loading and ϕ_F is the phase angle of the blade-rate harmonic of the propeller loading.

The phase angles corresponding to the orientation of the screen in the tunnel are defined by Equation (1) and have already been given. The phase angles of the blade-rate component of thrust and torque are measured with respect to the upward vertical in the propeller disk and the reference line of the propeller blade. Similarly, the phase angles for the four-cycle wake and the side forces and bending moments are related to the upward vertical.

Figure 15 indicates the horizontal and vertical bearing forces for the eight propellers, Figure 16 shows the horizontal and vertical bending

moments, and Figures 17 and 18 respectively present the corresponding phase angles for the bearing forces and bending moments. These angles are defined in the same manner as described previously, keeping in mind that z + 1 is used as the order of harmonic instead of blade-rate (z = number of blades).

DISCUSSION

As pointed out in the introduction, the main purpose of this investigation was to determine the effect of pitch on the fluctuating forces and moments produced by a propeller while operating in a spatially nonuniform wake field. Since the problem of determining the effects of changes in propeller geometry on the propeller vibratory forces concerns designers of marine propellers, a correlation of the experimental data is presented in terms of propeller design concepts. First, however, the present results are compared with the measured data of Boswell and Miller.[1]

The one Boswell-Miller case which permits comparison is their experiment with Propeller 4118 (P/D = 1.077; A_E/A_o = 0.6). The nondimensionalized unsteady thrust and torque (nondimensionalized by using the steady design thrust and torque, respectively) for this model at a design advance coefficient J_A equal to 0.83 were 0.45 and 0.36, respectively. The steady design thrust coefficient K_T was 0.15. The corresponding results for Propeller 4591 (P/D = 1.08; A_E/A_o = 0.54) for K_T = 0.15 were approximately 0.48 and 0.37 for the nondimensional thrust and torque, respectively. The corresponding advance coefficient for this case was J = 0.77, and the average torque coefficient, 10 K_Q, was equal to 0.29. Since the comparison indicates that the unsteady thrust and torque coefficients for the two propellers were nearly the same, it is concluded that the selection of commercially available propellers was indeed adequate for this investigation.

From the standpoint of designers of marine propellers, let us now examine the present experimental data for trends in the amplitude of the various unsteady forces and moments for a range of typical ship propulsion conditions.

A marine screw propeller is usually designed for a particular ship. The basic data which characterizes the ship are the wake survey in the propeller plane and the resistance of the hull, including an estimate of the interaction coefficients (thrust deduction and wake fraction). The resistance data, thrust deduction, and wake fraction can be represented as a thrust loading coefficient which usually varies only slightly with ship speed. For a given speed or operating point, the thrust loading coefficient

$$C_{Th} = \frac{8}{\pi} \cdot \frac{K_T}{J^2} = \frac{8}{\pi} \left(\frac{T}{\rho V_A^2 D^2} \right) \tag{3}$$

is a constant. Equation (3) yields a quadratic relationship between K_T and J which can be plotted on a graph along with the propeller open-water characteristics. The intersection gives the operating point. This concept of the ship operating point was used to evaluate the effect of changing pitch on the design of a propeller in terms of the unsteady propeller forces produced when the propeller operates in a wake.

The four values of thrust loading coefficient considered were selected to cover the range of typical ship operating conditions, namely, 0.51, 1.02, 1.53, and 2.04. These yield K_T/J^2 values equal to 0.2, 0.4, 0.6, and 0.8, respectively. In addition to showing the open-water characteristics of the propellers evaluated in this investigation, Figure 2 contains plots of the four constant-thrust coefficients, or ship operating characteristic curves. For a given C_{Th}, the intersections with propeller characteristics indicate a change in J versus pitch. Since C_{Th} is usually given at a particular speed, the change in J with pitch indicates the change in shaft speed. Obviously, the higher the pitch, the lower the shaft speed and, conseq ently, the higher the J. From the J for a given C_{Th} and a particular propeller (and, in this case, a particular pitch) the corresponding unsteady forces can be read from Figures 11-18. These data and those for steady thrust and torque were used to develop Figures 19-27. Figure 19 illustrates the effects of the changes

in pitch on propeller performance, and the other curves demonstrate the effect of pitch on the six components of the unsteady propeller forces.

It appears, somewhat intuitively, from the velocity diagram in Figure 28 that as the pitch is increased, the unsteady thrust should decrease while the unsteady torque should increase with increasing pitch. Figures 19-23 confirm this intuition. Note that as the pitch increases K_T, K_Q, and J increase. These changes result in changes in propeller efficiency, as illustrated in Figure 19 for K_T/J^2 equal to 0.2 and 0.6. Therefore, tradeoffs with efficiency and potential improvement in alternating thrust by way of increasing pitch must be evaluated in a design problem. Fortunately, in the case of pitch variation, the higher efficiencies were obtained with the higher pitched propellers for the low values of the steady thrust loading coefficient. Moreover, the effect of pitch on the alternating forces was not as large for the higher values of the steady thrust loading coefficient and, consequently, the higher efficiency designs at the lower pitch ratios constitute the proper design selections.

Figures 22 and 23 present the unsteady torque results. The coefficient used in Figure 22 ($\tilde{K}_Q/J^2$) was selected both because it did not contain the shaft speed and because it was the coefficient considered by Boswell and Miller.[1] The data in Figure 22 show that for a given ship speed or thrust loading coefficient (K_T/J^2), the unsteady torque increased with pitch ratio. This result contradicts the Boswell-Miller analytical predictions[1] which were computed by using an early version of the SIT program.[2] However, the result is consistent with what was indicated by the simple study of the velocity diagram given above. Figure 23 shows that the ratio of the unsteady torque divided by the steady torque tended to decrease slightly with increasing pitch-diameter ratio at a constant thrust coefficient.

The alternating side forces did not show significant changes with pitch, as illustrated in Figures 24 and 25. The bending moments decreased with increasing pitch, as shown in Figures 26 and 27.

These data indicate that in general, the higher the pitch in a given design problem, the greater the improvement that can be realized in alternating propeller thrust. However, such decreases are not significant from the design viewpoint because as far as efficiency is concerned the optimum design will yield a near-optimum pitch with respect to alternating force production. Moreover, changes in the unsteady forces contributed by skew and/or warp distributions are much more significant than the changes discussed herein.[1,4,6]

SUMMARY AND CONCLUSIONS

The six components of unsteady loading were measured experimentally for a series of three-bladed stock propellers that differed only in pitch. The unsteady forces and moments were produced by operating the propellers behind three- and four-cycle wake screens. The results lead to the following conclusions:

1. The unsteady thrust decreased with increasing pitch at a constant thrust loading coefficient.

2. The unsteady torque as described by the coefficient $\tilde{K}_Q/J^2$ increased with increase in pitch at a constant thrust loading coefficient. However, the ratio of unsteady-to-steady torque tended to decrease slightly with increasing pitch-diameter ratio at a constant thrust loading coefficient.

3. The side forces nondimensionalized by the steady thrust did not vary significantly for the various pitch ratios at a constant thrust loading coefficient.

4. The bending moments decreased with increasing pitch at a constant thrust loading coefficient.

5. In general, the results indicate that the higher the pitch in a given design problem, the greater the decrease in alternating propeller thrust that can be realized. However, it is not a practicable alternative to adjust P/D ratio as a means of decreasing alternating thrust for three reasons:

(a) as far as efficiency is concerned, optimum designs will yield near-optimum pitch ratios with regard to alternating thrust production; (b) the unsteady torque increases with pitch; and (c) other changes in geometry, e.g., skew and/or warp, have been found to result in much greater changes in the alternating forces produced by propellers than were measured in this investigation.

Figure 1 - Typical Shape of the Propeller Series
(Illustrated by Propeller 4592, P/D = 1.25)

Figure 2 - Open-Water Characteristics of the Pitch Series Propellers

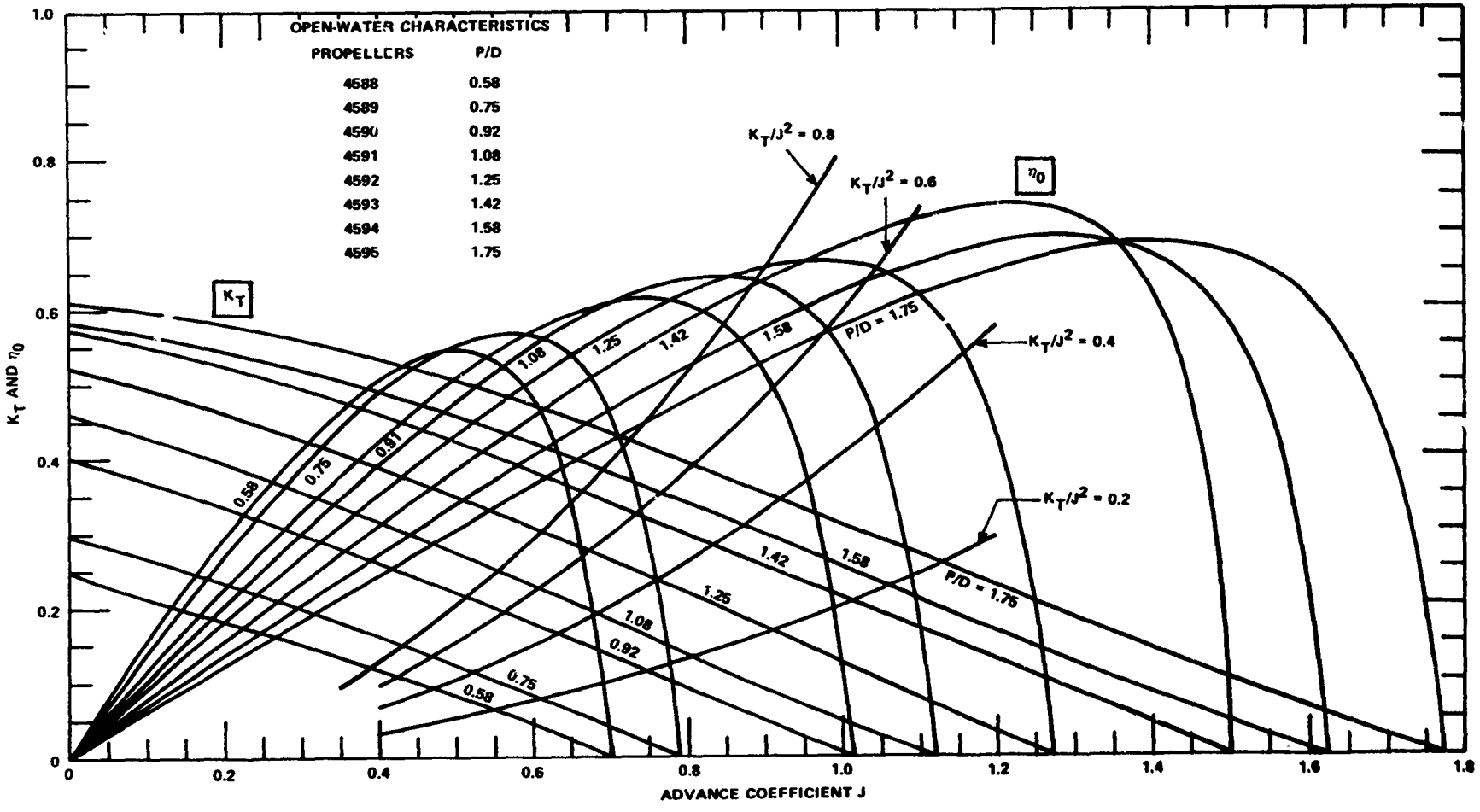

Figure 2a - Thrust Coefficient K_T and Efficiency η_0

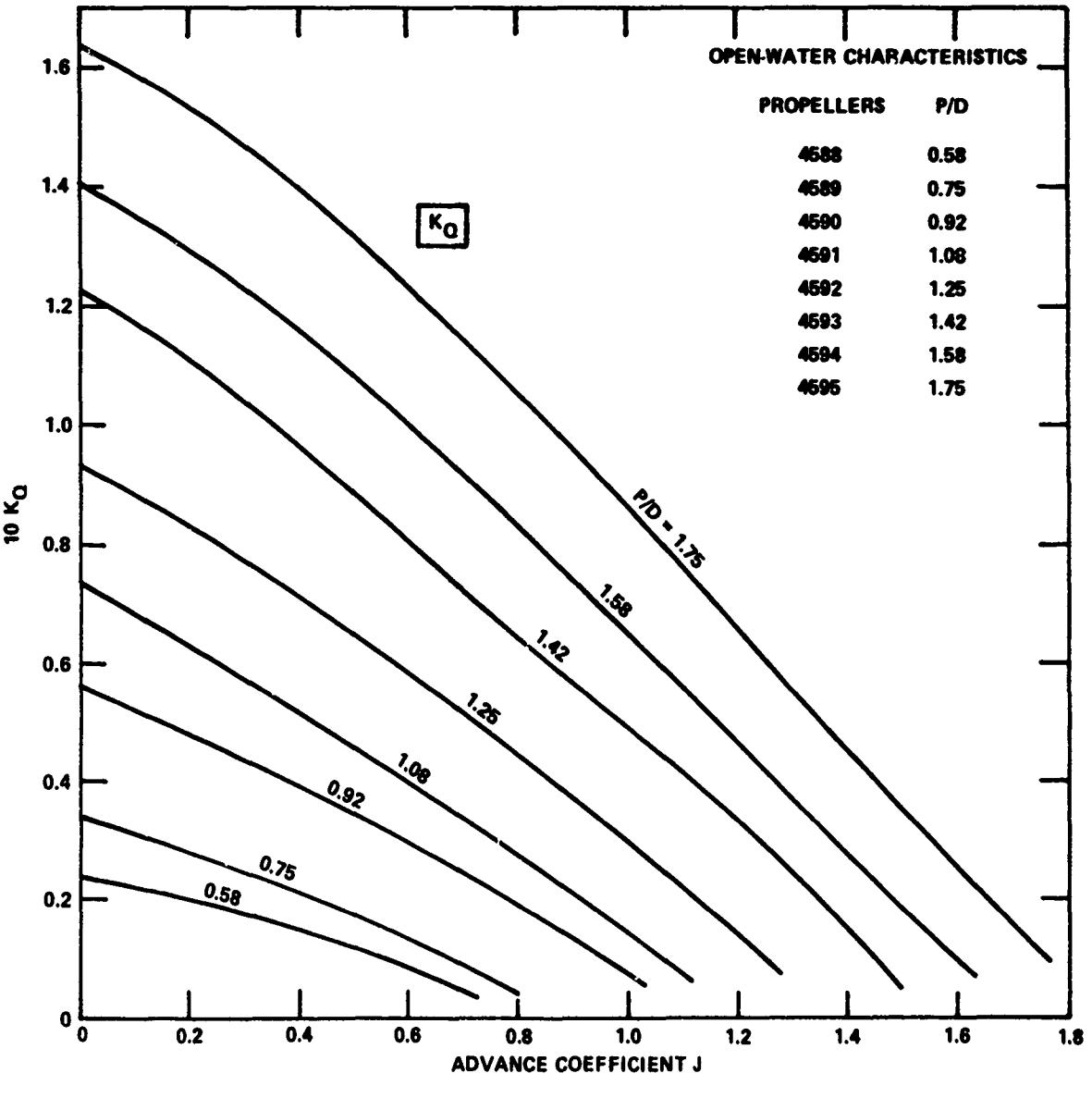

Figure 2b - Torque Coefficient 10 K_Q

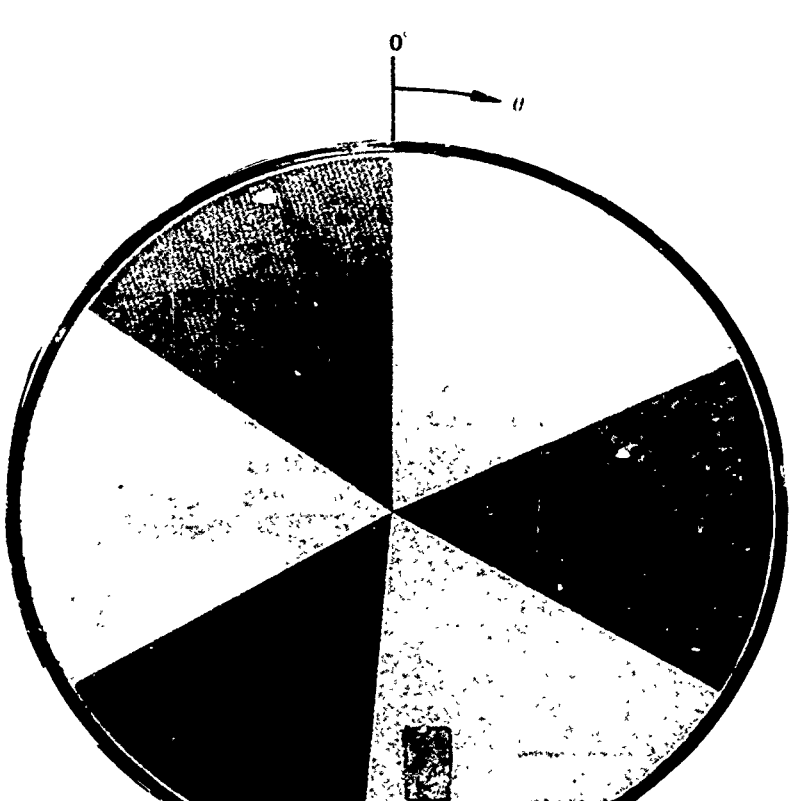

Figure 3 - Three-Cycle Wake Screen

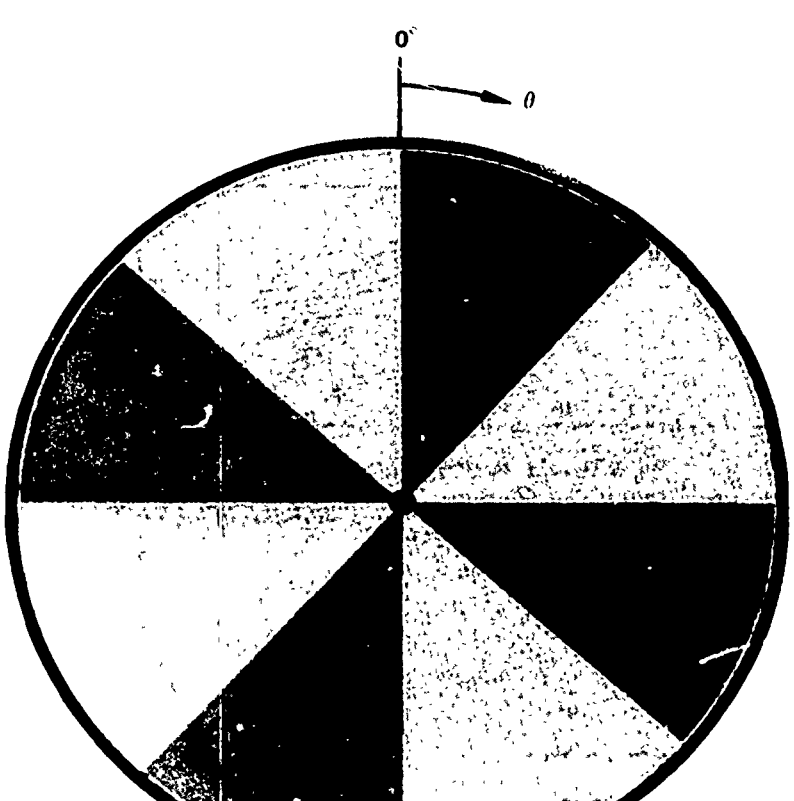

Figure 4 - Four-Cycle Wake Screen

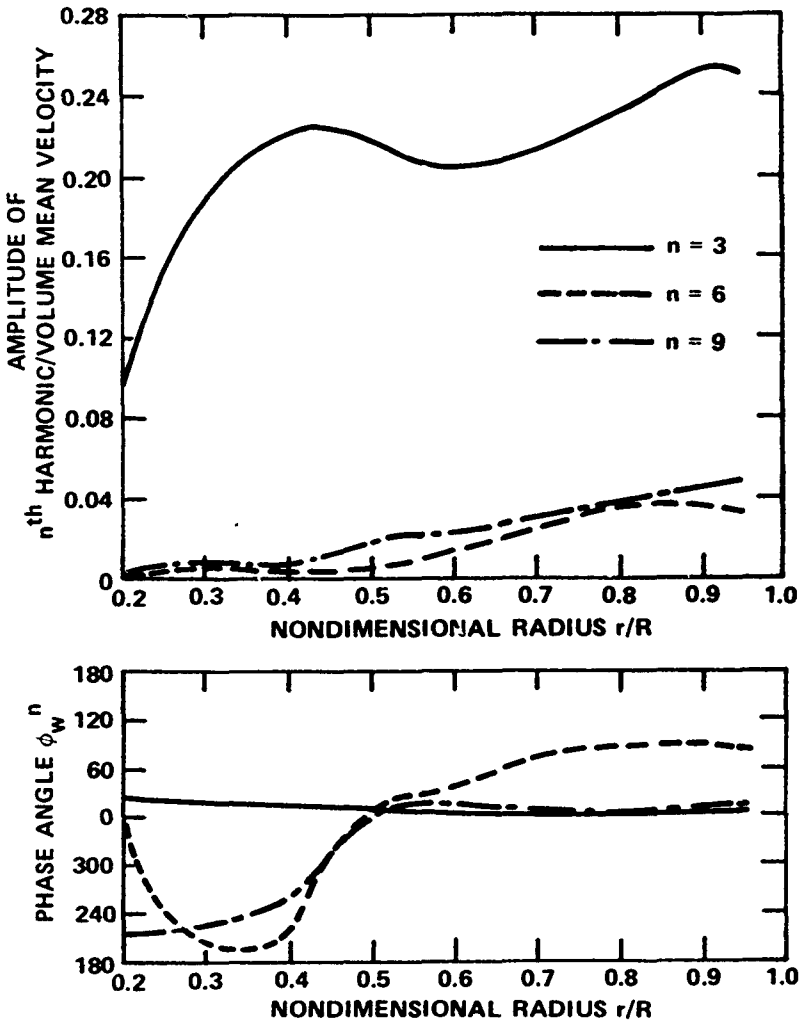

Figure 5 - Harmonic Content of Three-Cycle Wake

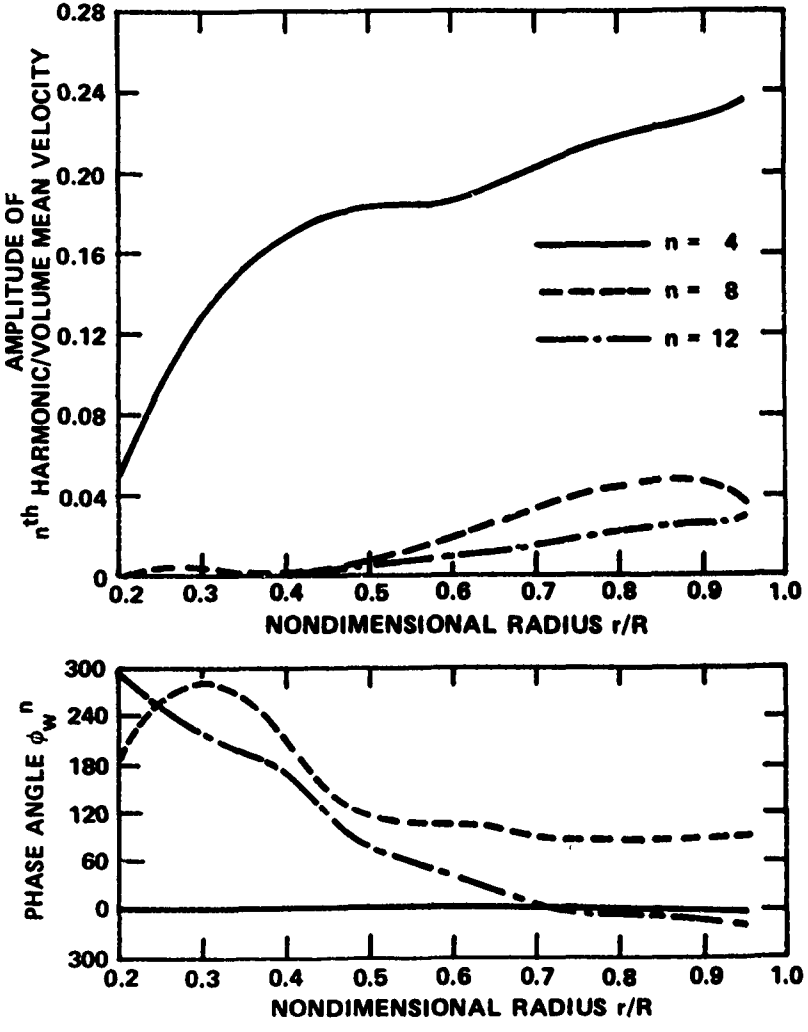

Figure 6 - Harmonic Content of Four-Cycle Wake

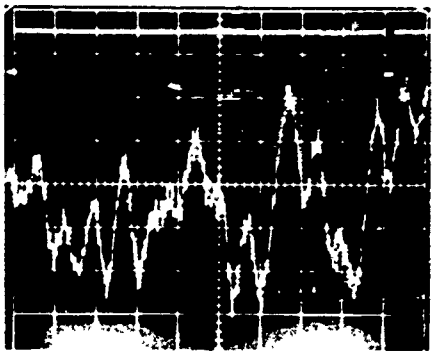

THRUST

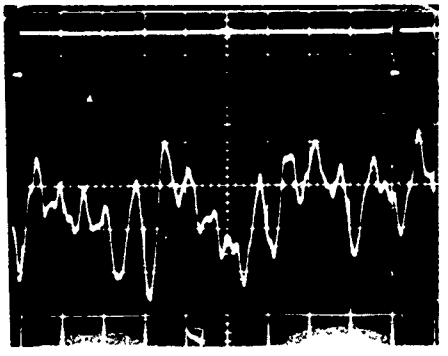

TORQUE

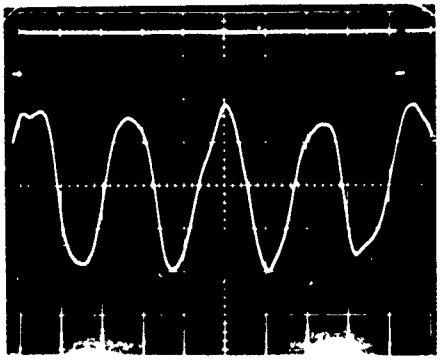

BENDING MOMENT 1

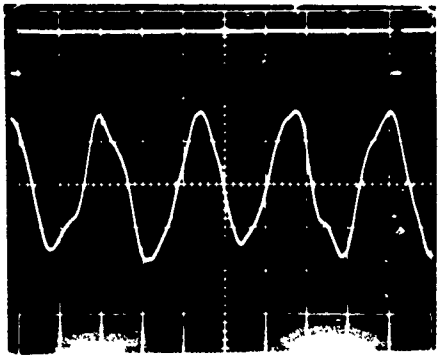

BENDING MOMENT 2

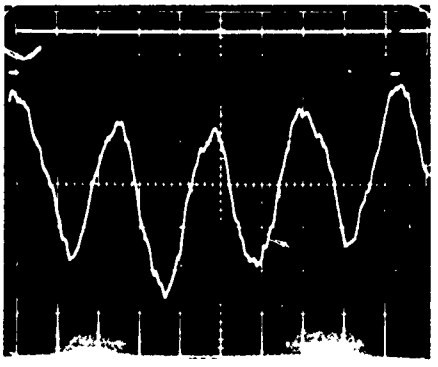

SIDE FORCE 1

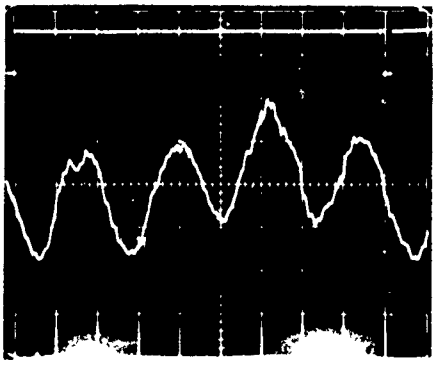

SIDE FORCE 2

Figure 7 - Typical Signals in Three-Cycle Wake

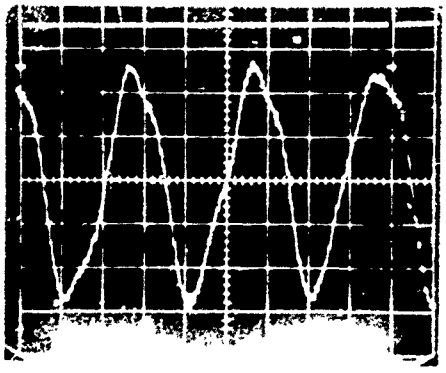

THRUST

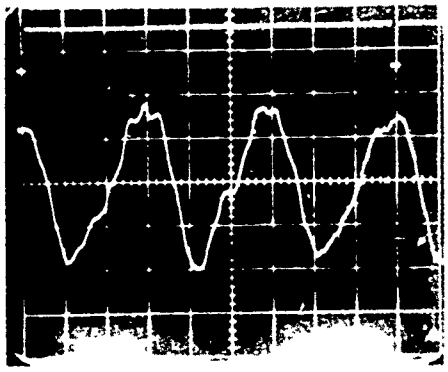

TORQUE

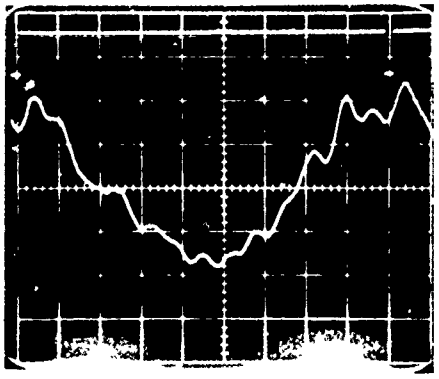

BENDING MOMENT 1

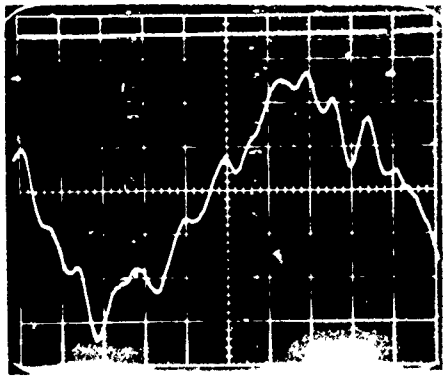

BENDING MOMENT 2

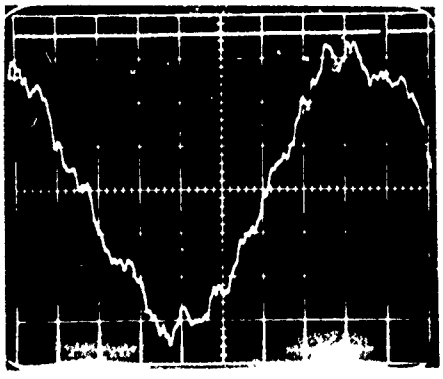

SIDE FORCE 1

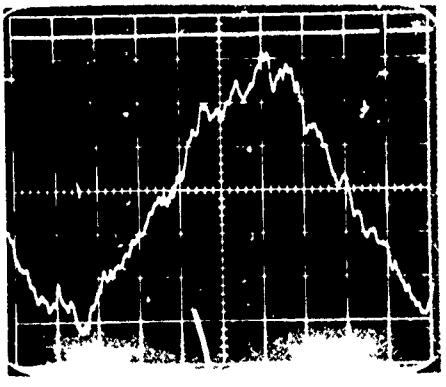

SIDE FORCE 2

Figure 8 - Typical Signals in Four-Cycle Wake

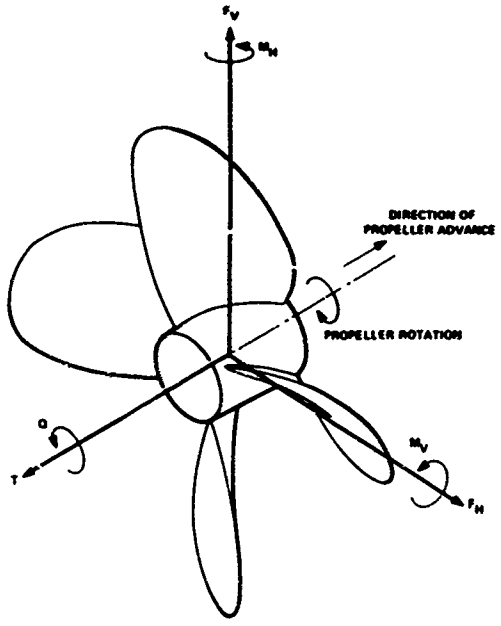

Figure 9 - Forces and Moments Acting on Propeller

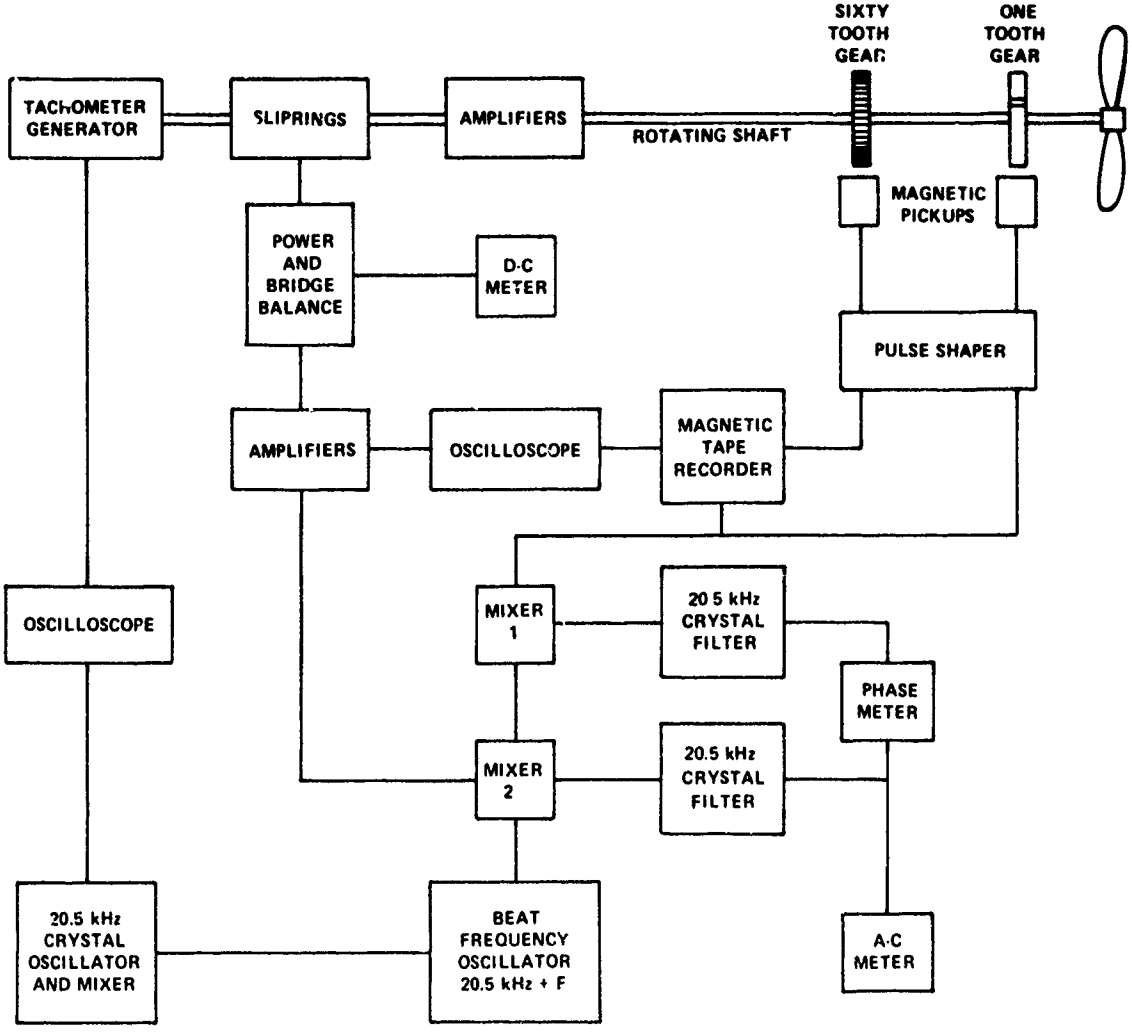

Figure 10 - Details of the Instrumentation

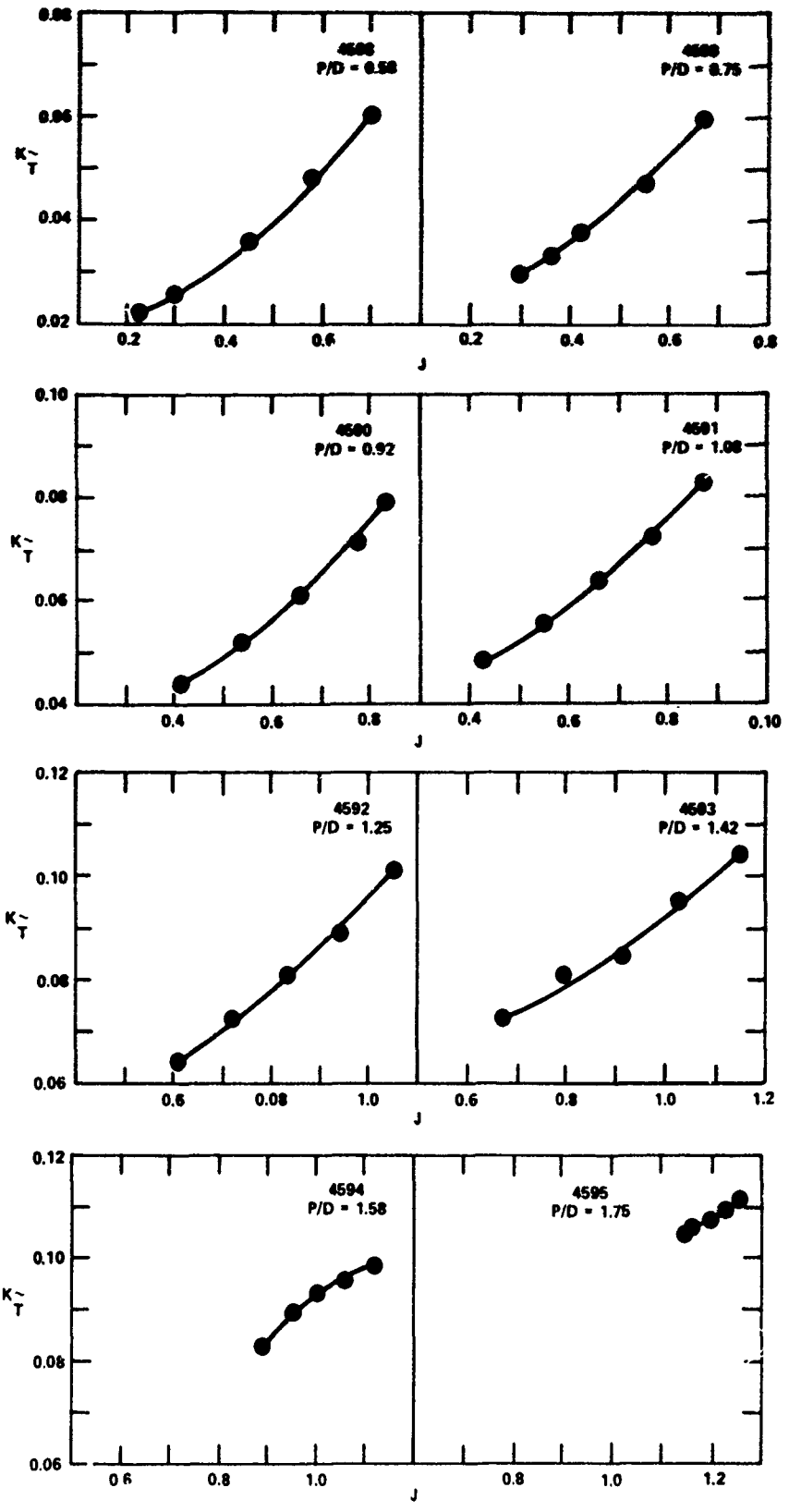

Figure 11 - Unsteady Thrust

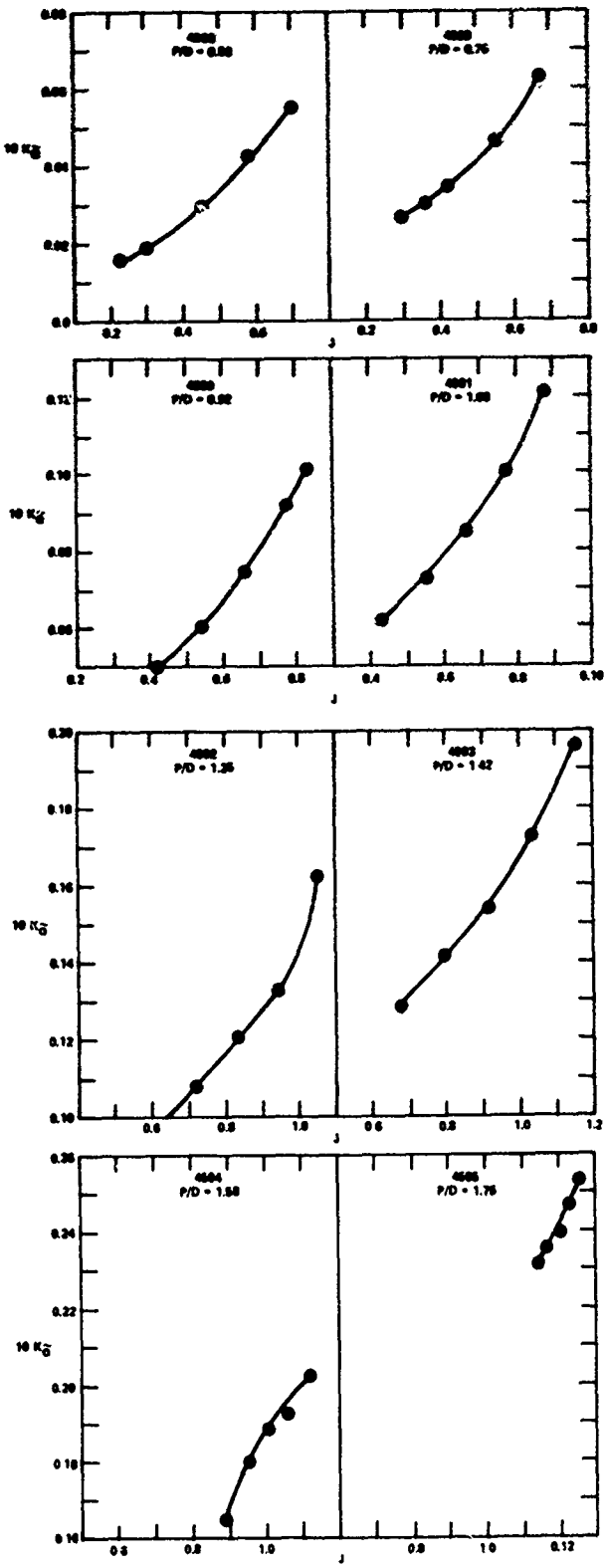

Figure 12 - Unsteady Torque

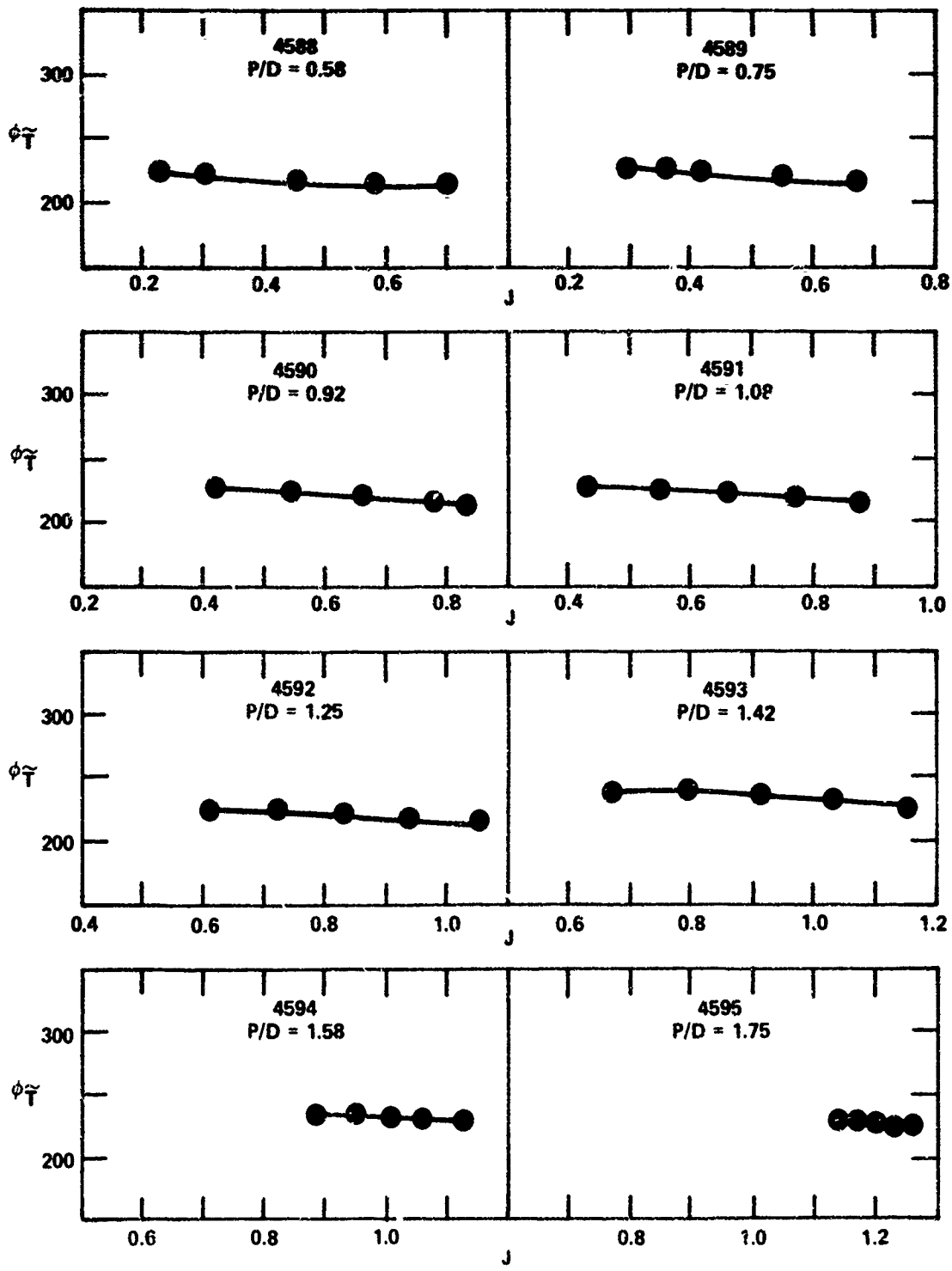

Figure 13 - Unsteady Thrust Phase Angles

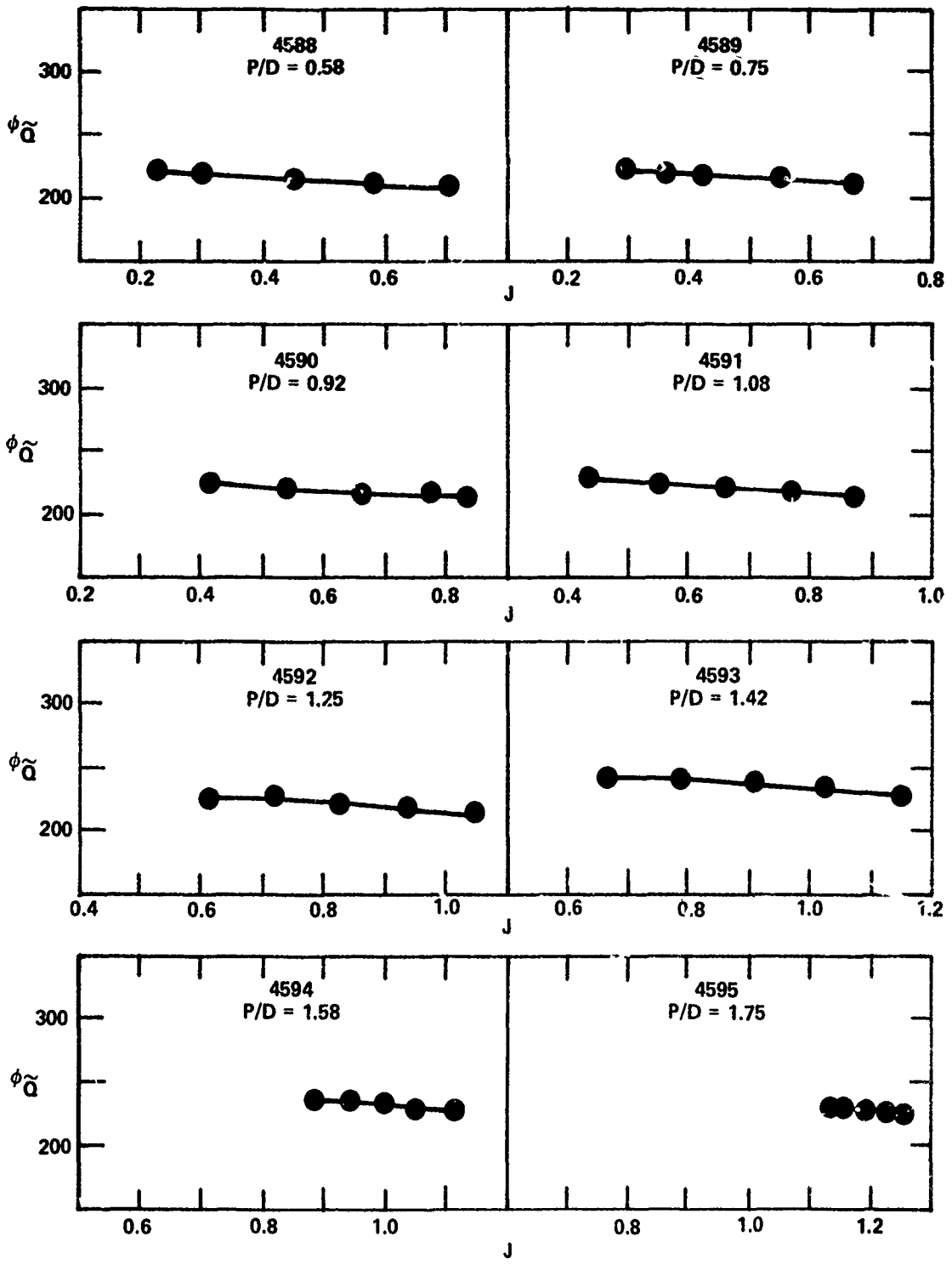

Figure 14 - Unsteady Torque Phase Angles

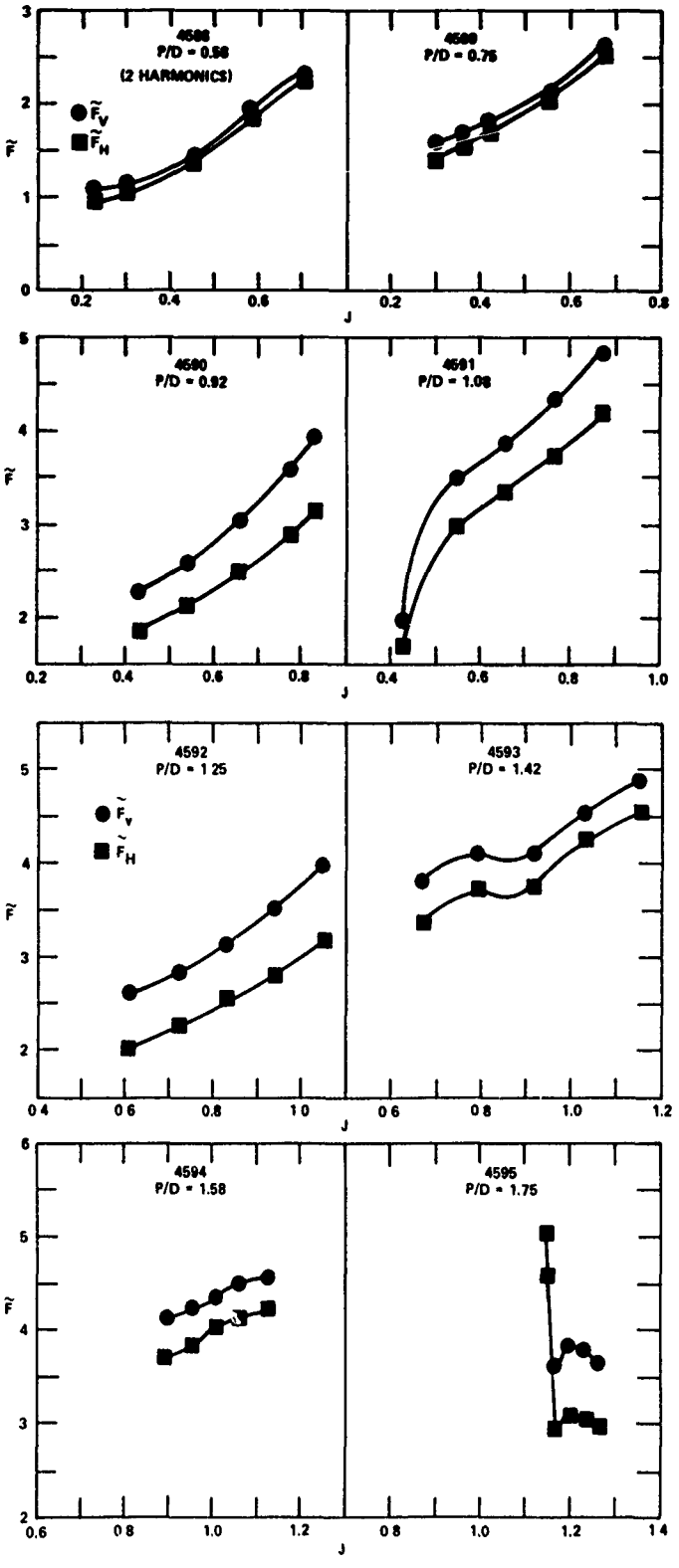

Figure 15 - Horizontal and Vertical Bearing Forces

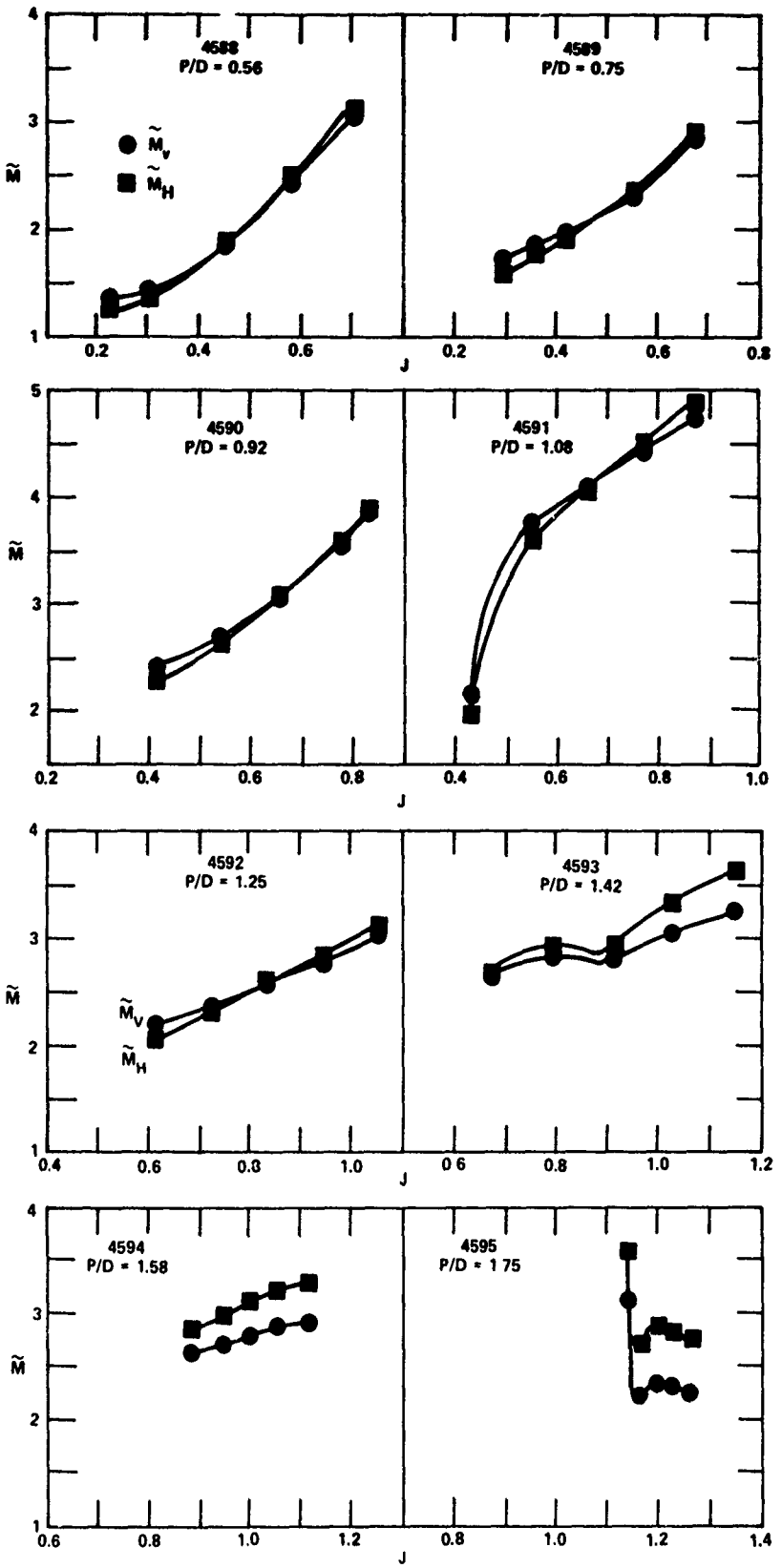

Figure 16 - Horizontal and Vertical Bending Moments

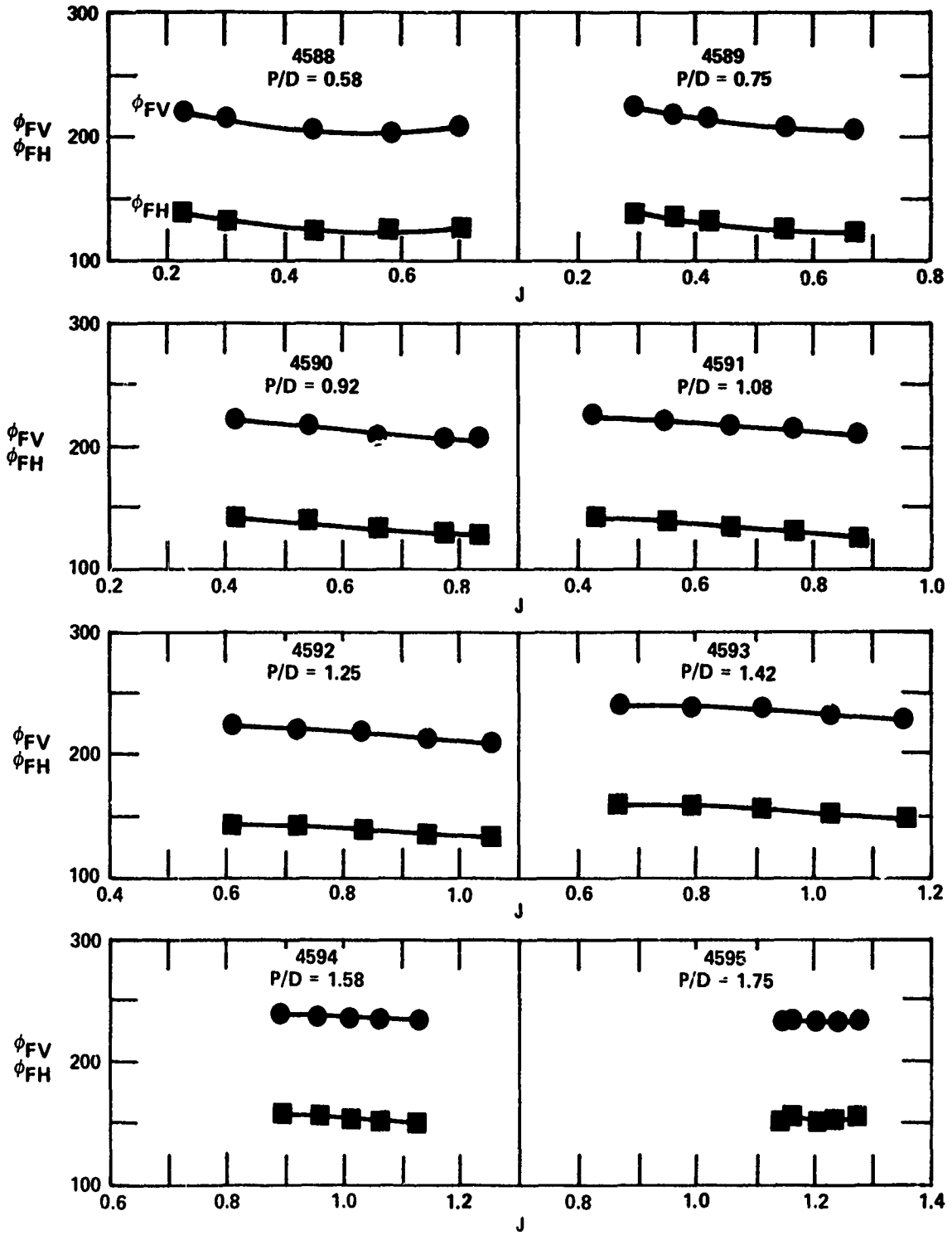

Figure 17 - Horizontal and Vertical Bearing Force Phase Angles

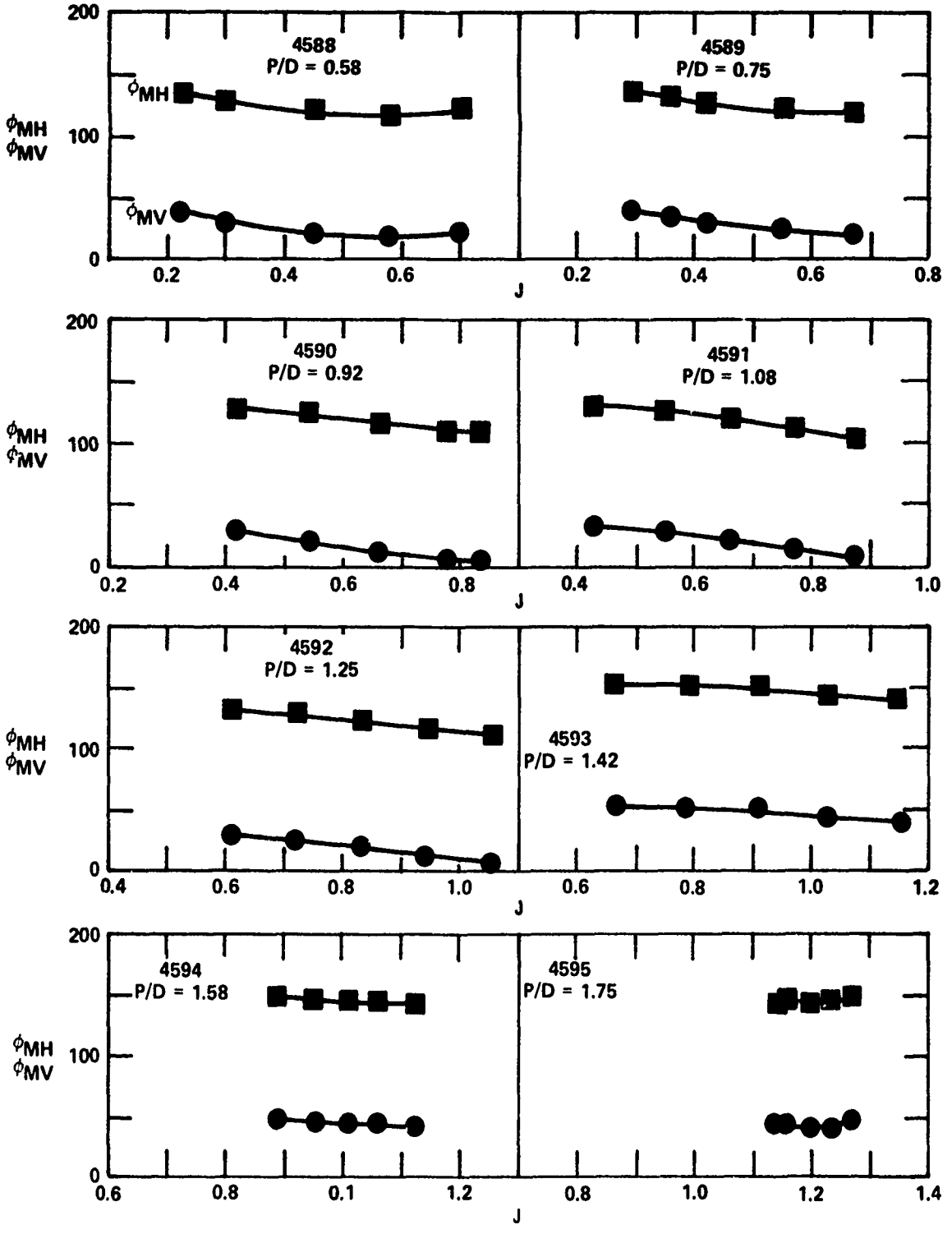

Figure 18 - Horizontal and Vertical Bending Moment Phase Angles

Figure 19 - Changes in Efficiency, Shaft Speed, Blade Frequency, Thrust, and Torque with Change in Pitch-to-Diameter Ratio for Constant Thrust Coefficient

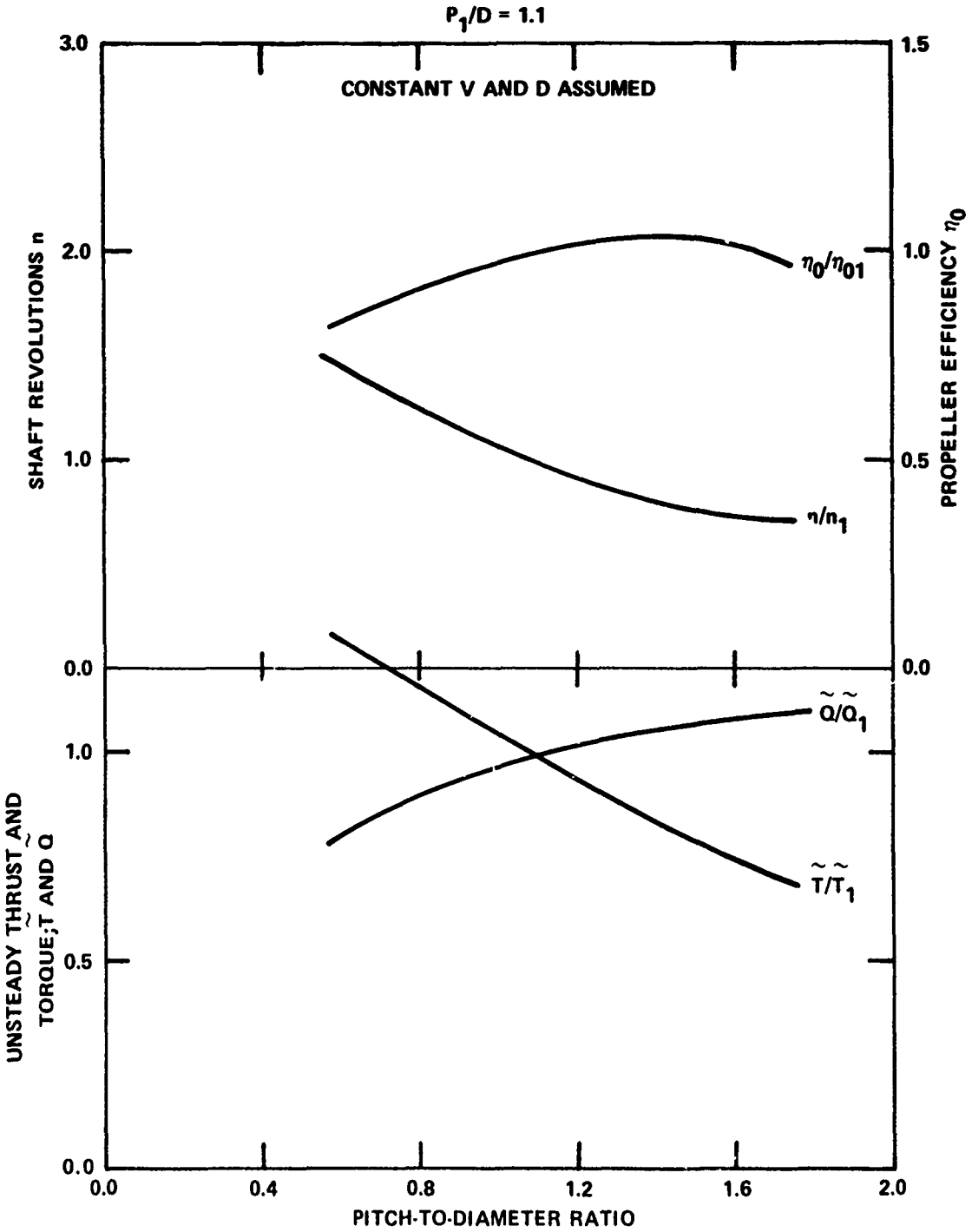

Figure 19a - For $C_{Th} = 0.509$

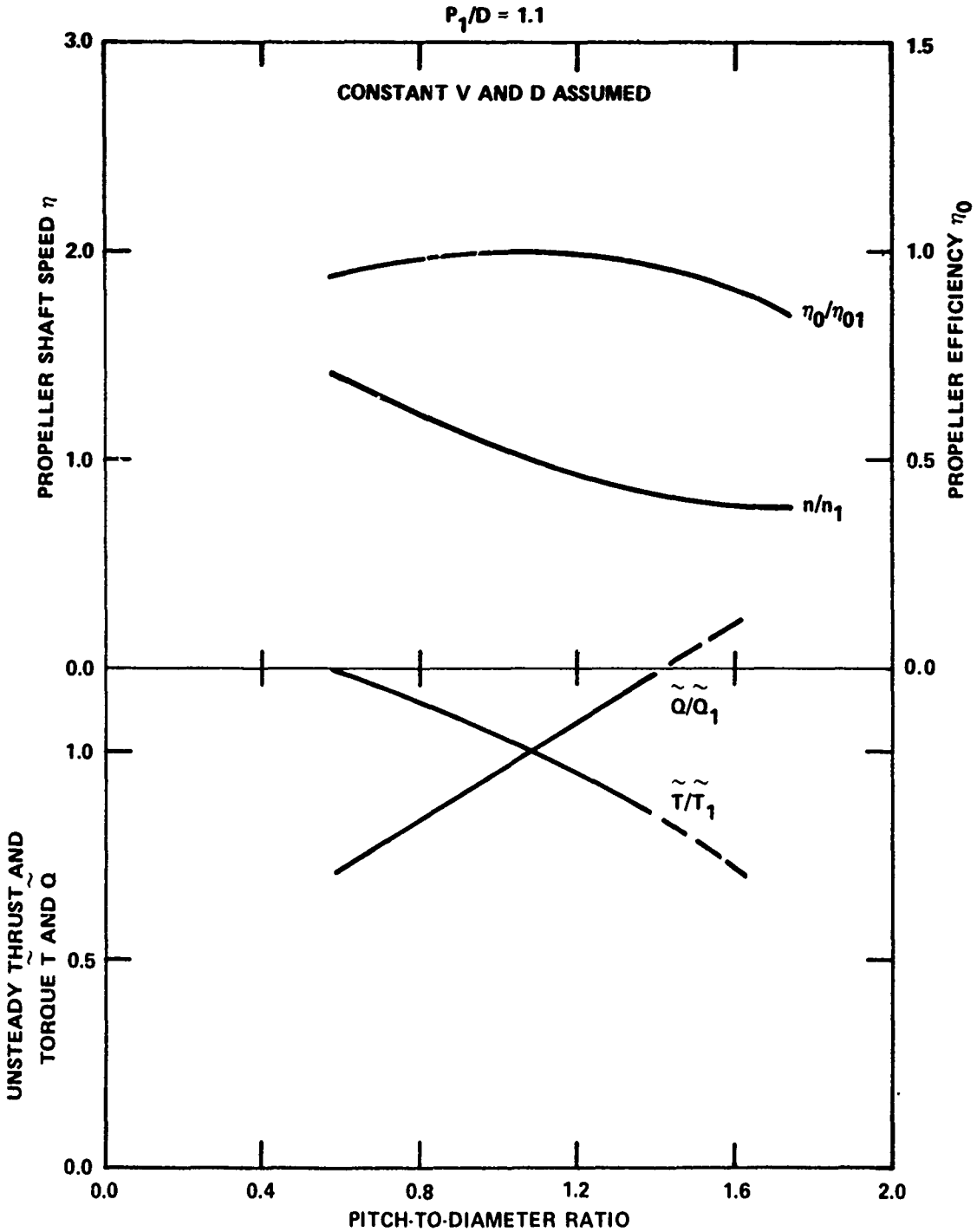

Figure 19b - For C_{Th} = 1.53

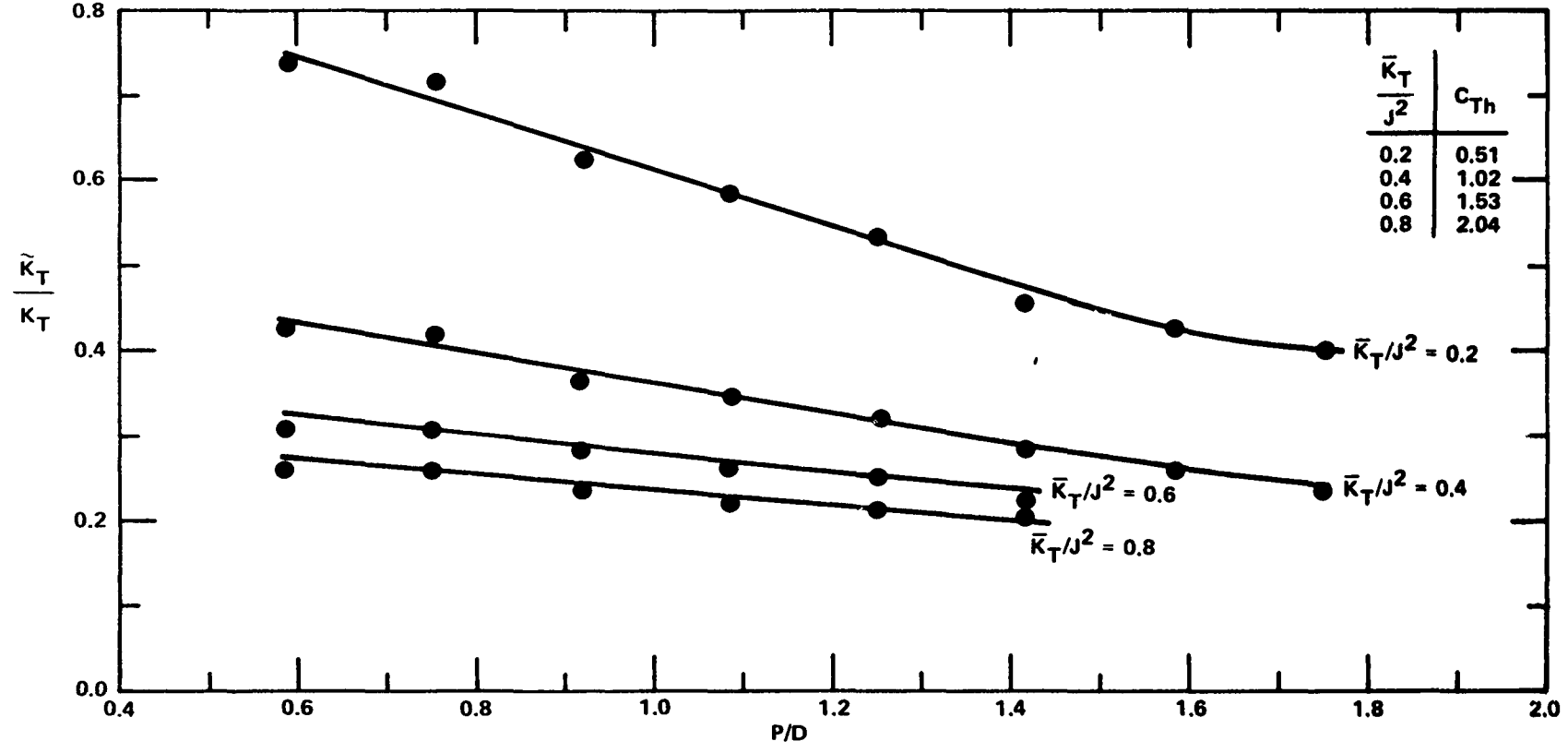

Figure 20 - Effect of Pitch Ratio on the Unsteady Thrust Divided by Steady Thrust

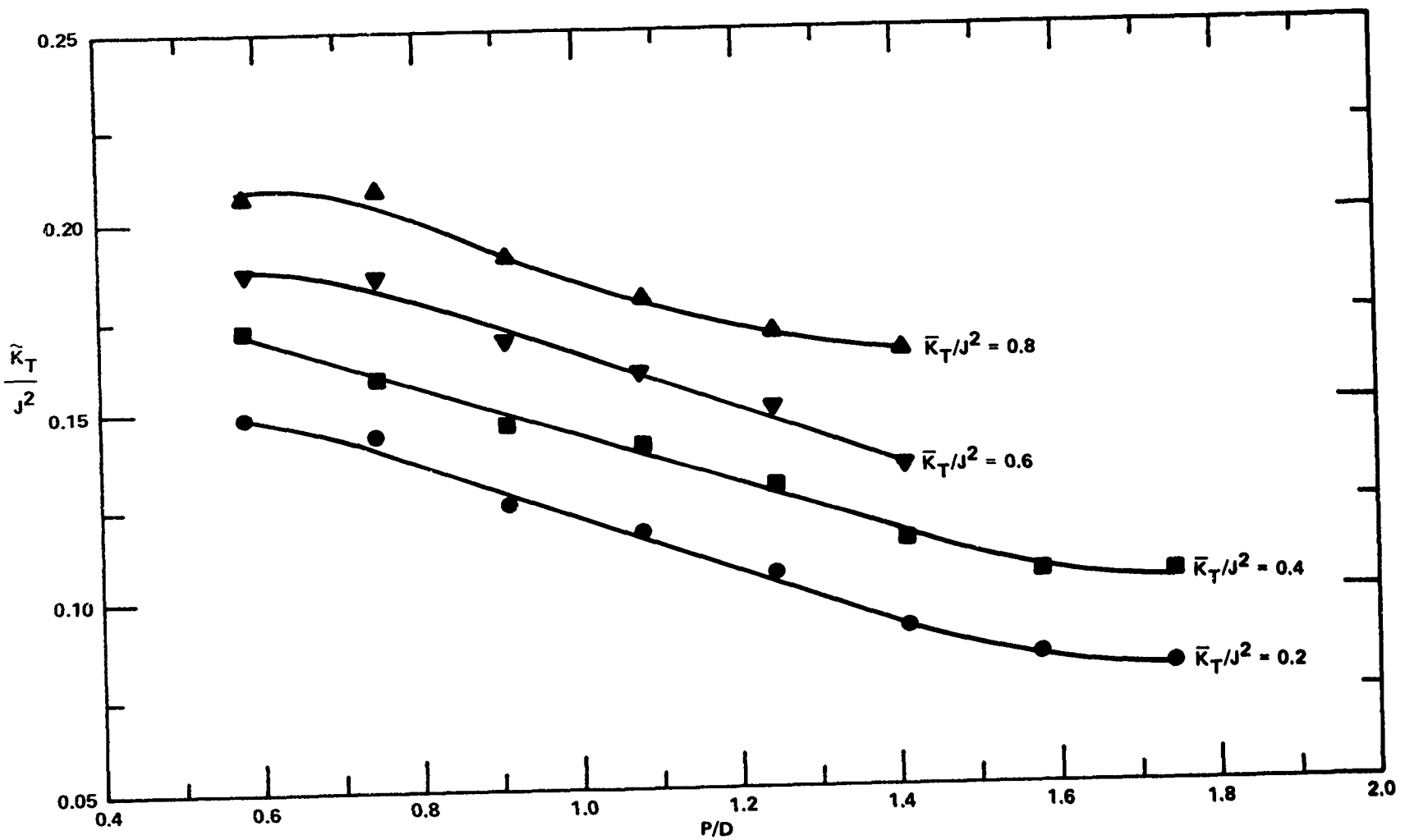

Figure 21 - Effect of Pitch Ratio on the Unsteady Thrust Divided by J^2

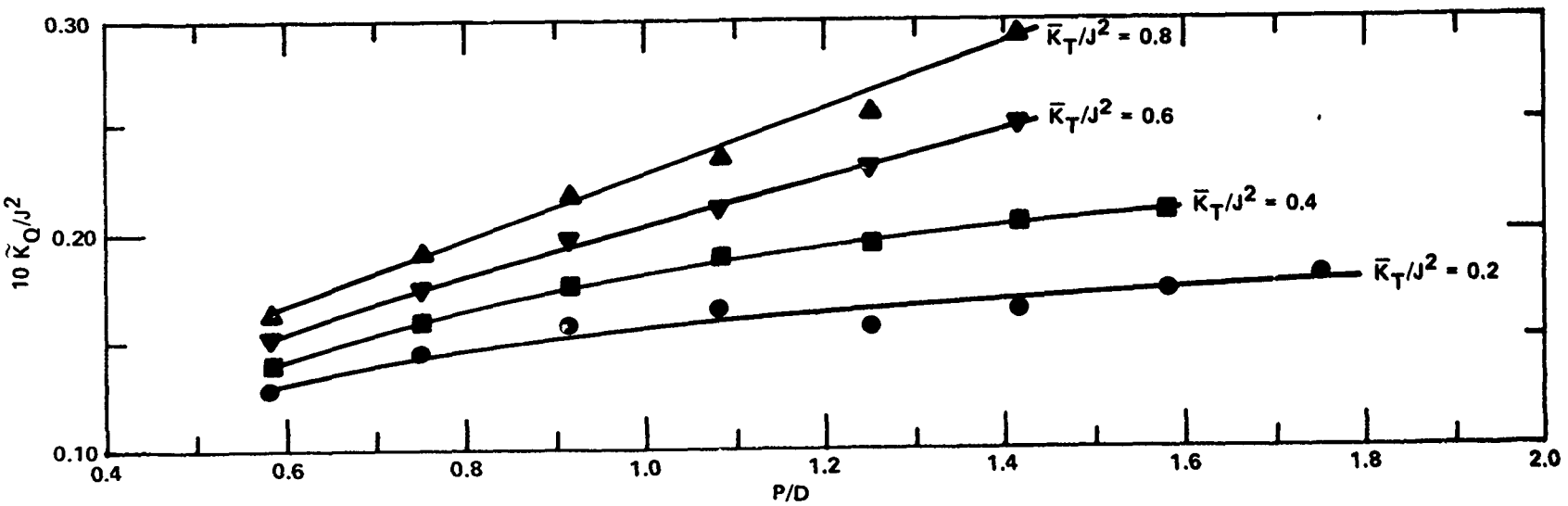

Figure 22 - Effect of Pitch Ratio on the Unsteady Torque Divided by J^2

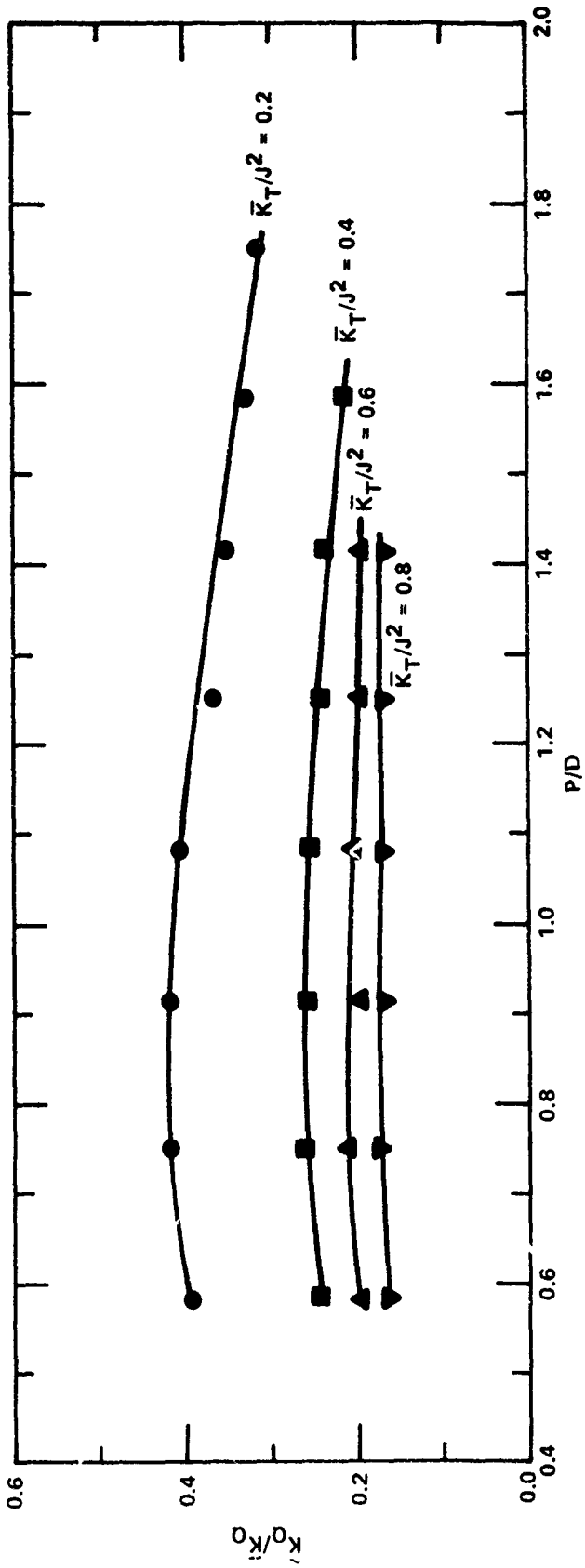

Figure 23 - Effect of Pitch Ratio on the Unsteady Torque Divided by Steady Torque.

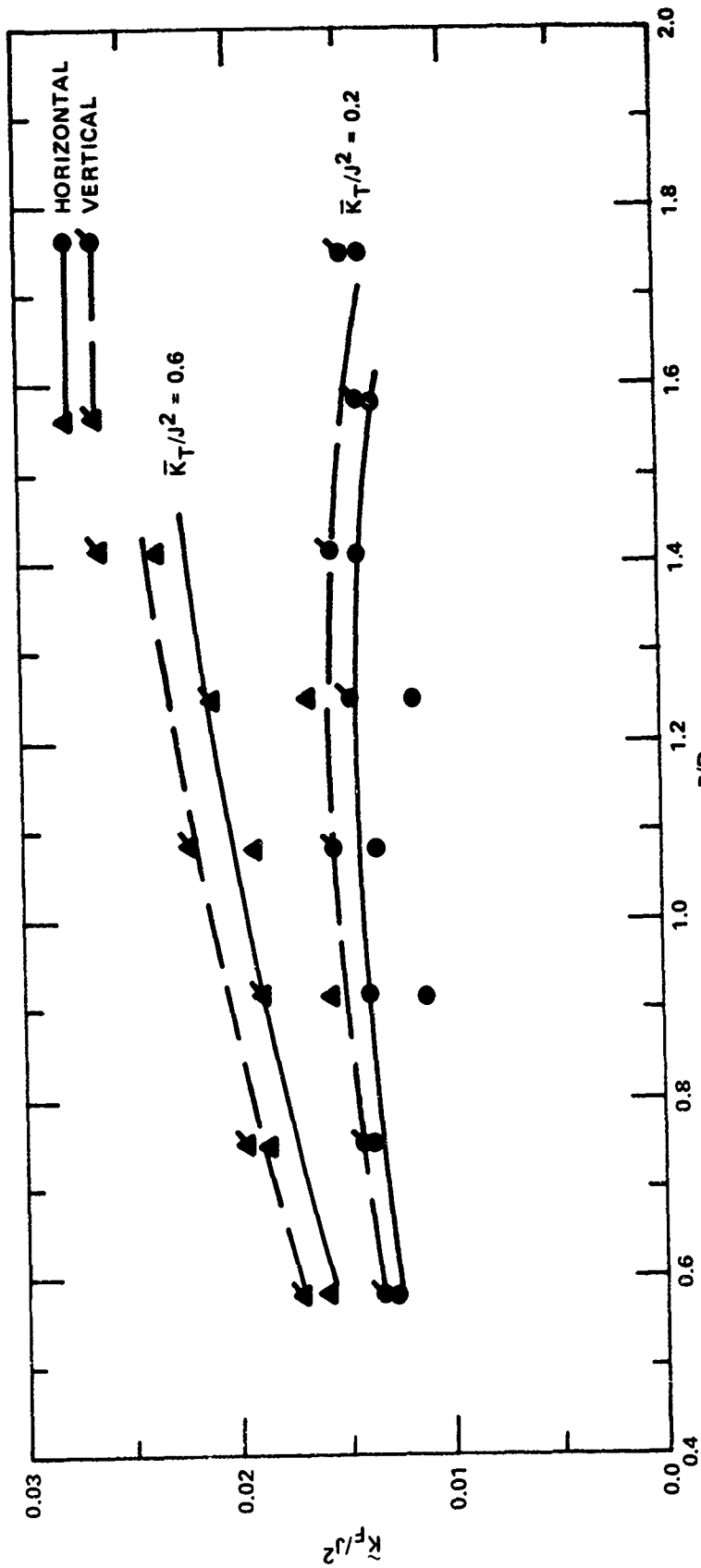

Figure 24 - Effect of Pitch Ratio on the Side Forces Divided by J^2

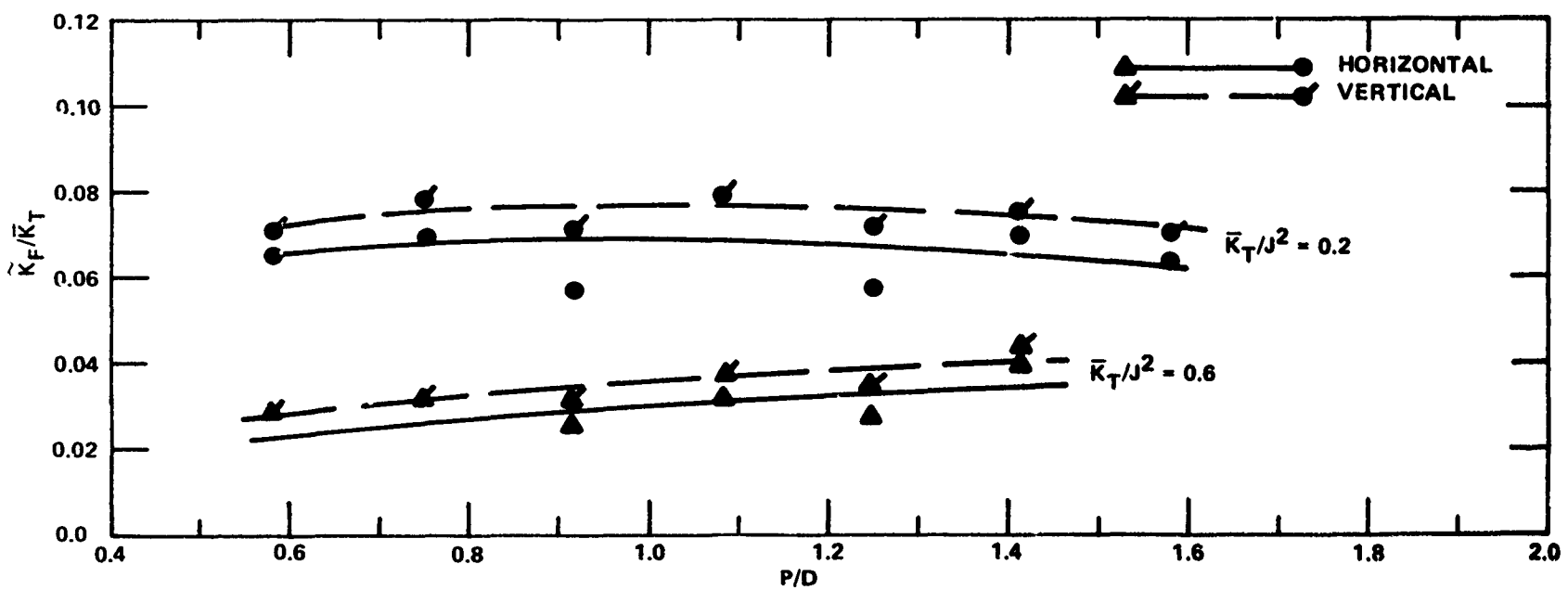

Figure 25 - Effect of Pitch Ratio on the Side Forces Divided by Steady Thrust

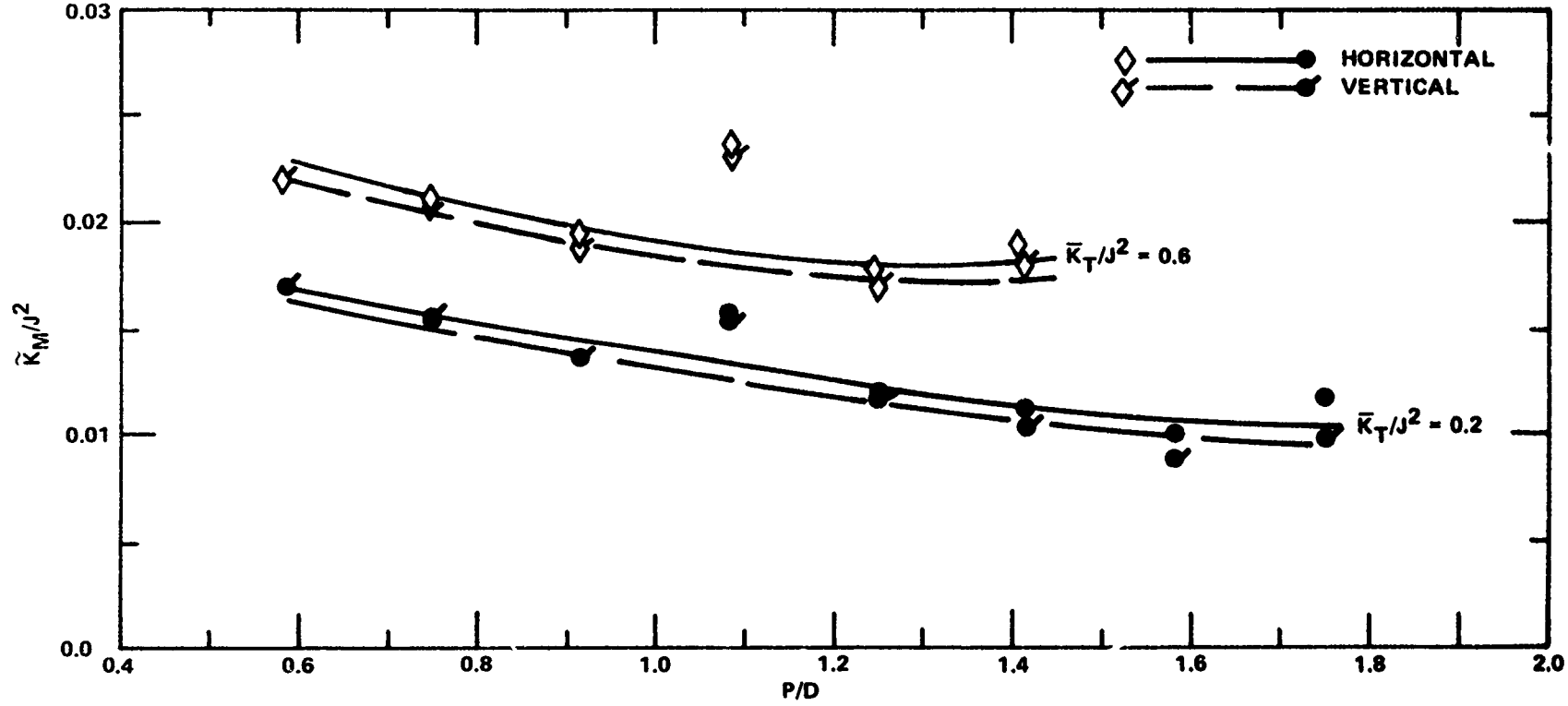

Figure 26 - Effect of Pitch Ratio on the Bending Moment Divided by J^2

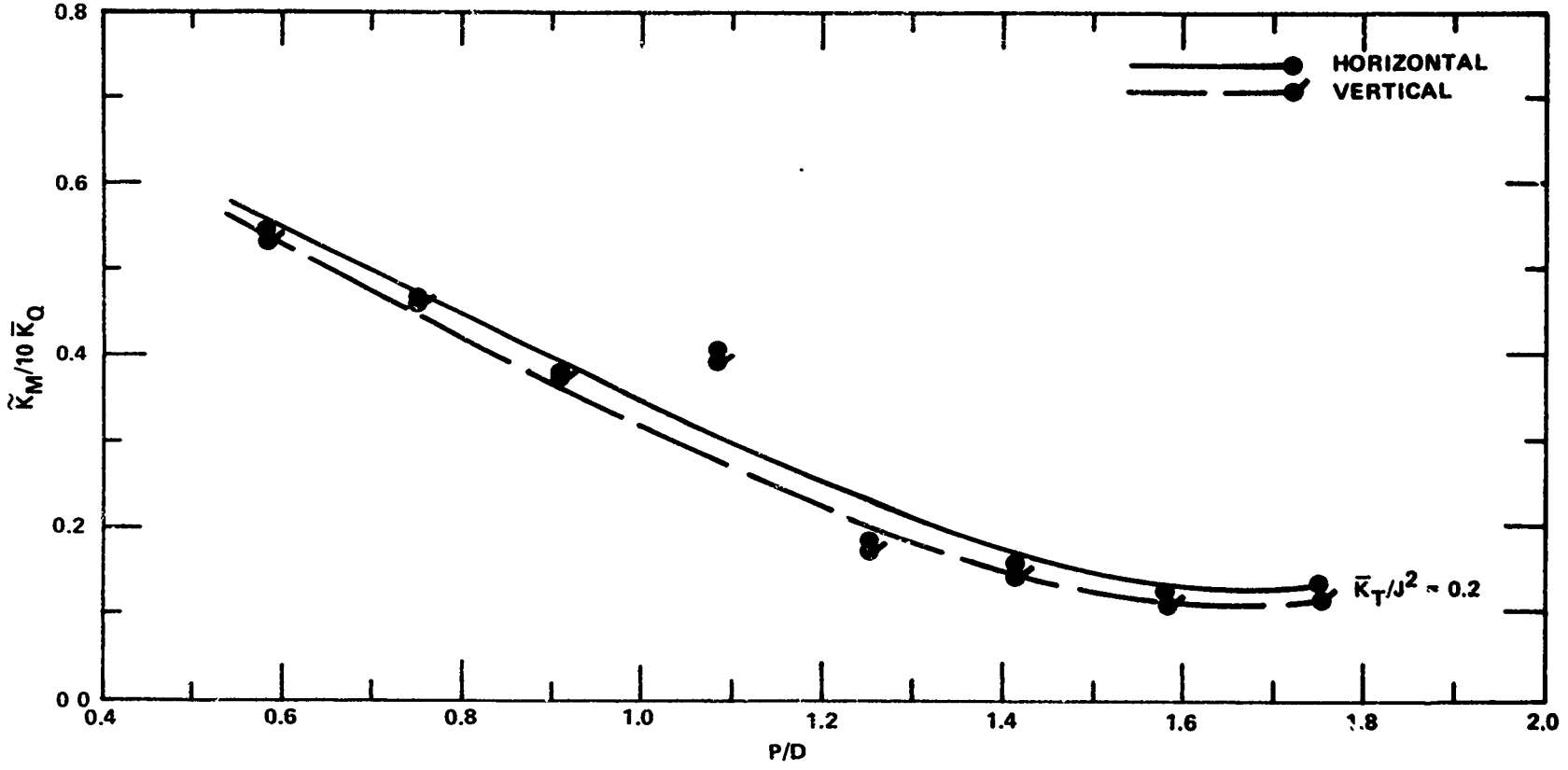

Figure 27 - Effect of Pitch Ratio on the Bending Moment Divided by Steady Torque

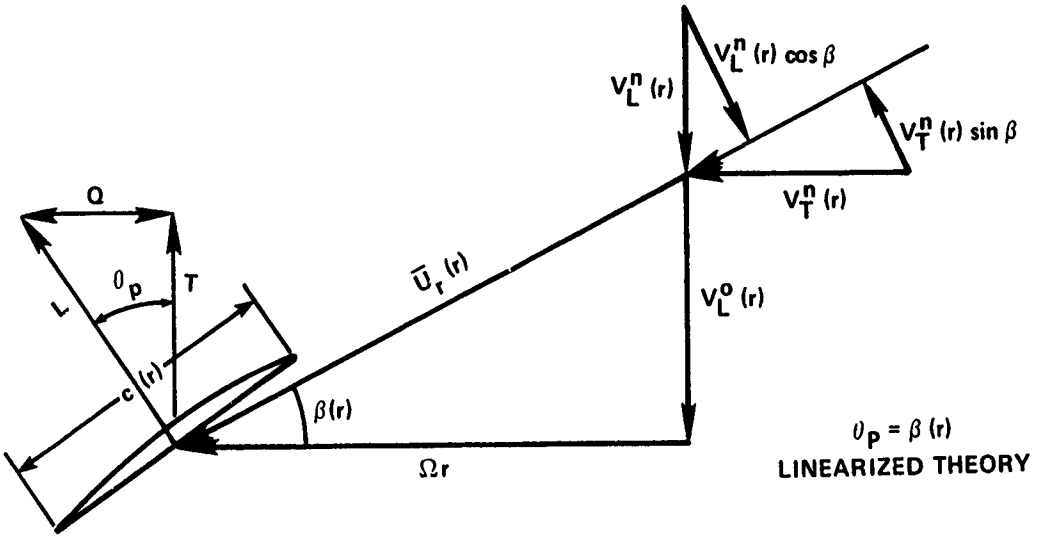

Figure 28 - Velocity Diagram

TABLE 1 - GEOMETRIC CHARACTERISTICS* OF STOCK PROPELLERS 4588, 4589, 4590, 4591, 4592, 4593, 4594, AND 4595
(Data are the Average Measurements for the Eight Michigan M-P Series)

Diameter (D) mm	305
Number of Blades Z	3
Expanded Area Ratio A_E/A_0	0.54
Blade Thickness Fraction BTF	0.36
Hub Diameter Ratio (cylindrical hub)	0.2
Rake	0
Skew	0
P/D = 0.58, 0.75, 0.92, 1.08, 1.25, 1.42, 1.58, 1.75	

r/R	c/D*
0.2	0.272
0.3	0.317
0.4	0.365
0.5	0.406
0.6	0.437
0.7	0.434
0.8	0.403
0.9	0.325
1.0	0.0

*The data is an average of measurements of the eight propellers.

TABLE 2 - HARMONIC CONTENT OF THREE-CYCLE WAKE

n	$\frac{V_L^n(0.25\ R)}{V_{VM}}$	$\phi_w^n(0.25\ R)$	$\frac{V_L^n(0.35\ R)}{V_{VM}}$	$\phi_w^n(0.35\ R)$	$\frac{V_L^n(0.45\ R)}{V_{VM}}$	$\phi_w^n(0.45\ R)$	$\frac{V_L^n(0.55\ R)}{V_{VM}}$	$\phi_w^n(0.55\ R)$
1	0.015	242.0	0.025	200.1	0.023	194.2	0.014	201.8
2	0.009	334.3	0.012	97.8	0.021	96.7	0.023	86.5
3	0.147	19.4	0.210	14.6	0.222	10.0	0.211	4.6
4	0.007	111.4	0.018	92.2	0.024	79.4	0.028	67.2
5	0.006	345.1	0.014	3.3	0.011	6.5	0.003	340.8
6	0.003	200.8	0.005	208.7	0.001	286.5	0.008	24.3
7	0.001	304.3	0.002	249.8	0.004	225.3	0.005	226.1
8	0.003	320.0	0.004	320.1	0.003	338.9	0.002	54.6
9	0.007	222.7	0.007	234.4	0.004	326.2	0.015	12.0
10	0.002	307.2	0.000	188.3	0.006	111.7	0.013	103.4
11	0.000	348.9	0.001	100.7	0.002	121.0	0.003	139.2
12	0.001	348.9	0.003	321.3	0.002	321.1	0.002	89.8
13	0.002	131.3	0.002	111.6	0.001	96.3	0.000	10.9
14	0.000	68.1	0.001	307.2	0.002	246.6	0.003	228.2
15	0.001	171.2	0.001	145.6	0.002	162.9	0.002	165.2

n	$\frac{V_L^n(0.65\ R)}{V_{VM}}$	$\phi_w^n(0.65\ R)$	$\frac{V_L^n(0.75\ R)}{V_{VM}}$	$\phi_w^n(0.75\ R)$	$\frac{V_L^n(0.85\ R)}{V_{VM}}$	$\phi_w^n(0.85\ R)$	$\frac{V_L^n(0.95\ R)}{V_{VM}}$	$\phi_w^n(0.95\ R)$
1	0.011	235.3	0.016	253.1	0.023	257.4	0.021	264.9
2	0.019	82.7	0.012	86.7	0.010	66.1	0.014	19.9
3	0.207	0.7	0.220	0.4	0.244	1.9	0.252	2.1
4	0.025	53.6	0.019	33.7	0.014	12.9	0.009	324.0
5	0.010	231.1	0.021	235.1	0.026	237.4	0.019	227.7
6	0.017	59.6	0.030	81.0	0.036	88.7	0.033	83.7
7	0.009	256.0	0.015	277.2	0.013	297.6	0.015	302.9
8	0.004	38.8	0.009	8.8	0.015	2.6	0.010	355.4
9	0.026	10.4	0.033	4.9	0.041	7.6	0.048	13.7
10	0.015	79.5	0.016	50.3	0.008	63.1	0.003	179.2
11	0.005	195.6	0.009	221.2	0.007	217.7	0.010	266.9
12	0.008	82.5	0.015	74.0	0.016	71.9	0.013	73.6
13	0.002	223.1	0.004	230.3	0.008	281.4	0.014	310.5
14	0.001	250.8	0.003	24.5	0.005	63.4	0.011	36.9
15	0.003	116.5	0.006	79.3	0.011	61.5	0.019	46.8

TABLE 3 - HARMONIC CONTENT OF FOUR-CYCLE WAKE

n	$\frac{V_L^n(0.25\ R)}{V_{VM}}$	$\phi_w^n(0.25\ R)$	$\frac{V_L^n(0.35\ R)}{V_{VM}}$	$\phi_w^n(0.35\ R)$	$\frac{V_L^n(0.45\ R)}{V_{VM}}$	$\phi_w^n(0.45\ R)$	$\frac{V_L^n(0.55\ R)}{V_{VM}}$	$\phi_w^n(0.55\ R)$
1	0.041	151.4	0.035	156.9	0.025	171.5	0.018	199.7
2	0.029	170.6	0.035	166.2	0.026	183.2	0.024	244.6
3	0.019	110.8	0.038	89.3	0.030	80.5	0.011	47.9
4	0.095	1.4	0.154	2.5	0.180	4.0	0.186	5.2
5	0.023	114.2	0.040	115.1	0.034	113.3	0.017	107.7
6	0.006	66.9	0.008	325.4	0.006	323.8	0.009	335.8
7	0.001	167.7	0.002	17.7	0.007	90.1	0.012	3.4
8	0.002	274.3	0.002	272.8	0.003	208.9	0.012	112.3
9	0.001	6.9	0.001	291.1	0.003	249.3	0.005	241.7
10	0.002	61.2	0.002	368.4	0.007	215.9	0.015	278.4
11	0.001	71.7	0.000	6.1	0.002	77.2	0.003	253.3
12	0.003	236.1	0.003	201.0	0.002	232.8	0.006	56.5
13	0.001	221.2	0.001	252.4	0.002	128.3	0.002	283.8
14	0.002	128.6	0.003	148.2	0.001	214.2	0.002	312.9
15	0 001	211.3	0.003	231.2	0.003	239.5	0.004	274.2

n	$\frac{V_L^n(0.65\ R)}{V_{VM}}$	$\phi_w^n(0.65\ R)$	$\frac{V_L^n(0.75\ R)}{V_{VM}}$	$\phi_w^n(0.75\ R)$	$\frac{V_L^n(0.85\ R)}{V_{VM}}$	$\phi_w^n(0.85\ R)$	$\frac{V_L^n(0.95\ R)}{V_{VM}}$	$\phi_w^n(0.95\ R)$
1	0.017	220.5	0.014	218.5	0.010	195.4	0.007	152.9
2	0.030	265.4	0.023	260.0	0.011	215.7	0.008	165.1
3	0.010	12.8	0.016	46.0	0.015	36.5	0.014	4.6
4	0.195	4.1	0.211	1.3	0.223	359.2	0.236	356.9
5	0.009	103.2	0.011	118.9	0.010	145.4	0.013	143.4
6	0.014	321.2	0.014	27.3	0.013	15.2	0.019	43.4
7	0.009	6.0	0.002	78.6	0.006	79.3	0.008	83.7
8	0.025	98.0	0.039	89.0	0.047	87.3	0.040	91.1
9	0.009	230.8	0.012	223.0	0.008	220.6	0.006	128.0
10	0.016	273.2	0.010	261.7	0.007	190.2	0.007	147.0
11	0.002	325.4	0.007	30.9	0.007	40.7	0.006	306.1
12	0.011	20.6	0.019	357.7	0.024	350.7	0.028	342.5
13	0.002	289.7	0.000	319.1	0.001	118.7	0.004	93.6
14	0.004	324.3	0.005	340.4	0.008	9.4	0.010	16.6
15	0.001	287.0	0.004	102.7	0.007	107.6	0.007	115.0

REFERENCES

1. Bosvell, R.J. and M.L. Miller, "Unsteady Propeller Loading - Measurement, Correlation with Theory, and Parametric Study," NSRDC Report 2625 (Oct 1968).

2. Tsakonas, S.,et al., "Correlation and Application of an Unsteady Flow Theory for Propeller Forces," Transactions of the Society of Naval Architects and Marine Engineers, Vol. 75, pp. 158-193 (1967).

3. Tsakonas, S.,et al., "An Exact Linear Lifting-Surface Theory for a Marine Propeller in a Nonuniform Flow Field," Stevens Institute of Technology DL Report 1509 (Feb 1972).

4. Cumming, R.A.,et al., "Highly Skewed Propellers," Transactions of the Society of Naval Architects and Marine Engineers," Vol. 80, pp. 98-135 (1972).

5. Valentine, D.T. and F.J. Dashnaw, "Highly Skewed Propellers for San Clemente Class Ore/Bulk/Oil Carrier Design Considerations, Model and Full-Scale Evaluation," Proceedings of the First Ship Technology and Research (STAR) Symposium, Washington, D.C. (Aug 1975).

6. Nelka, J.J., "Experimental Evaluation of a Series of Skewed Propellers with Forward Rake: Open-Water Performance, Cavitation Performance, Field-Point Pressures, and Unsteady Propeller Loading," DTNSRDC Report 4113 (Jul 1974).

7. Miller, M.L., "Experimental Determination of Unsteady Propeller Forces," Seventh ONR Symposium on Naval Hydromechanics, DR-148, pp. 255-289 (Aug 1968).

INITIAL DISTRIBUTION

Copies	
1	Chief of R&D, OCS, Army
1	Army Eng R&D, Ft. Belvoir
1	Army Trans R&D, Ft. Eustis
2	CHONR
	1 Fluid Dynamics (Code 438)
	1 Sys & Res Gp (Code 492)
1	NRL
1	ONR Boston
1	ONR Chicago
1	ONR Pasadena
1	ONR San Francisco
1	USNA
1	USNPGSCOL, Monterey
1	USNROTC
1	NAVWARCOL
1	NADC
1	NELC
1	NUC
1	NWC
1	NURDC
1	NCEL
15	NAVSEA
	1 SEA 031
	1 SEA 033
	1 SEA 035A
	2 SEA 037
	1 SEA 08
	3 SEA 09G32
	1 PMS-383
	1 PMS-389
	1 PMS-393
	1 PMS-396
	1 PMS-397
	1 PMS-399
1	NUSC

Copies	
1	NAVSHIPYD Bremerton
1	NAVSHIPYD Charleston
1	NAVSHIPYD Long Beach
1	NAVSHIPYD Philadelphia
1	NAVSHIPYD Portsmouth
8	NAVSEC
	1 SEC 6100
	2 SEC 6110
	1 SEC 6140B
	2 SEC 6144
	2 SEC 6148
1	NAVSEC Norfolk (Code 6660)
12	DDC
1	US MA
1	CMDT, USCOGARD
1	NASA College Park Attn: Sci & Tech Info, Acquisition Br
9	MARAD
	1 Ship Div
	1 Coord of Research
	1 Mr. R. Schubert
	1 Mr. R. Falls
	1 Mr. R.K. Kiss
	1 Mr. J.J. Nachtsheim
	1 Mr. F. Dashnaw
	1 Mr. Hammar
	1 Mr. C. Foltis
1	BUSTAND
1	Institute for Defense Analysis
1	Library of Congress
1	Merchant Marine Academy
1	National Science Foundation
1	Cal Inst of Tech
1	Catholic Univ

Copies

1 Colorado State Univ
Attn: Prof M. Albertson

1 Cornell Univ

1 Harvard Univ
Attn: Prof G. Birkhoff
Dept of Mathematics

2 JHU, Baltimore
1 Dept of Mechanics
1 Inst of Cooperative Research

1 Kansas State Univ
Attn: Prof D.A. Nesmith

1 Lehigh Univ
Attn: Fritz Lab Lib

7 MIT
Dept of Ocean Engineering
1 Prof P. Mandel
1 Prof J.E. Kerwin
1 Prof P. Leehey
1 Prof M. Abkowitz
1 Dr. J.N. Newman
1 Prof M. Landahl
1 Prof S. Widnall

3 New York Univ
Courant Institute
1 Prof A.S. Peters
1 Prof J.J. Stoker
1 Prof K.O. Frederick

1 Penn State U, ARL

2 Southwest Research Institute
1 Dr. H. Abramson
1 Applied Mechanics Review

2 Stanford Univ
1 Prof M. Van Dyke
1 Prof H. Ashley

1 Stanford Research Institute
Attn: Lib

1 State Univ of New York
Maritime College
1 Engineering Dept

Copies

3 Stevens Institute of Technology, Davidson Lab
1 Dr. J.P. Breslin
1 Dr. S. Tsakonas
1 Lib

1 Webb Institute of Naval Architecture
1 Prof E.V. Lewis
1 Prof C. Ridgely-Nevitt
1 Lib

1 Woods Hole Oceanographic Institute
Attn: Reference Room

1 Worcester Polytechnic Institute
Attn: Director

3 Univ of Calif, Berkeley
Naval Architecture Dept
1 Lib
1 Prof J.V. Wehausen
1 Prof J.R. Paulling

1 Univ of Connecticut
Attn: Prof V. Scottron

1 Univ of Illinois, College of Engr
Attn: Dr. J.M. Robertson

1 Univ of Iowa
Attn: Dr. Hunter Rouse

2 Univ of Iowa
1 Dr. L. Landweber
1 Dr. J. Kennedy

2 Univ of Michigan
Dept of Naval Architecture & Marine Engr
1 Dr. T.F. Ogilvie
1 Lib

1 Univ of Minnesota
St. Anthony Falls Hydraulic Lab
1 Director

1 Univ of Notre Dame
Dept of Mech Engr

Copies	
1	Univ of Washington Applied Physics Lab Attn: Director
1	AVCO, Lycoming Div., Washington
1	Baker Mfg, Evansville
1	Bethelehem Steel Corp. Sparrows Point Yard Attn: Mr. A. Haff, Tech Mgr
1	Boeing Aircraft AMS Div. Seattle
1	Bolt Beranek & Newman, Inc. Attn: Dr. N. Brown
1	Cambridge Acoustical Associates, Inc. Attn: Mr. M.C. Junger
1	Esso International Attn: Mr. R.J. Taylor Manager, R&D Tanker Dept.
1	General Dynamics, Electric Boat Attn: Mr. V. Boatwright, Jr.
2	Gibbs & Cox, Inc. 1 Tech Lib 1 Mr. Frank Butler
1	Grumman, Bethpage Attn: Mr. W. Carl
2	Hydronautics, Inc.
1	ITEK Corp, Vidya Div. Palo Alto
1	Lockheed Missiles and Space Sunnyvale 1 Dept 5701
1	Martin Co., Baltimore
1	McDonnell-Douglas Aircraft Corp. 1 Mr. John Hess
1	National Steel & Shipbldg Co.

Copies	
1	Newport News Shipbldg & DD Co. Attn: Technical Lib Dept
1	Puget Sound Bridge & Drydock Co., Seattle
1	George G. Sharp, Inc.
1	Sperry-Gyro Co. Attn: Mr. D. Shapiro (Mail Sta G2)
1	SNAME
1	Sun Shipbldg & DD Co.
1	Tectra Tech, Inc.
1	United Aircraft Hamilton Standard Div.
1	Rutgers Univ Mechanical and Aerospace Engineering Attn: Dr. R.H. Page

CENTER DISTRIBUTION

Copies	Code
1	1124
1	1500
1	1502
1	1504
1	1505
1	1506
1	1520
2	1521
2	1524
2	1528
1	1532
1	1540
1	1542

Copies		
15	1544	
1	1552	
1	1560	
1	1568	
2	1720.6	
1	1850	
1	19	
1	1962	
1	272	
1	274	
30	5214.1	Reports Distribution
1	5221	Library (C)
1	5222	Library (A)